A BRILLOUIN GAIN SPECTROMETER AND ITS EVALUATION BY THE STUDY OF SOME LIQUIDS

CHUNXIA FAN

A BRILLOUIN GAIN SPECTROMETER AND ITS EVALUATION BY THE STUDY OF SOME LIQUIDS

by

©Chunxia Fan, B.Sc.(Hons), M.Sc.

A thesis submitted to the School of Graduate

Studies in partial fulfilment of the

requirements for the degree of

Master of Science

Department of Physics

Memorial University of Newfoundland

August 1994

St.John's Newfoundland

ISBN 0-315-96079-5

Abstract

The construction and testing of a Brillouin gain spectrometer is discussed. The spectrometer employs a high power (150 mW) tunable dye laser and a low power (1.7 mW) stabilized HeNe laser in a pump-probe arrangement. Because of the small signal gain (1×10^{-5}), several noise reduction schemes were used to enhance the signal to noise ratio. The spectrometer was evaluated by studying the strongly scattering liquid CS_2 and the weakly scattering liquid CCl_4. Brillouin shifts and linewidths were accurately determined for both liquids. The high resolution of this instrument permitted measurement of the small asymmetry in the measured lineshapes. In CCl_4 we were able to observe the so-called Mountain mode and to confirm that CCl_4 can be modeled as a liquid exhibiting a single relaxation time.

Acknowledgements

I wish to thank my supervisors Dr.H.Kiefte and Dr. M.J.Clouter for their continuous encouragement, support and guidance. I also wish to express my sincere appreciation to Dr. Richard Goulding for his valuable help, guidance, discussion at every stage of this project and reviewing of this thesis.

I am grateful to Mr. H Clarke for his helping in electronics, Mr. O.Vazquez and Mr. C. Tulk for their helping in many aspects, such as computer, English, and useful discussions during my stay in the Physics department.

I would like to thank Memorial University of Newfoundland for awarding a Fellowship and offering a Teaching Assistantship.

Finally, my husband, Zhongxin, deserves my warmest appreciation for his understanding, support and encouragement.

Table of Contents

List of Tables

List of Figures

CHAPTER 1.

INTRODUCTION

1-1. Brillouin Scattering

The phenomenons of light scattered by sound waves was first predicted by Brillouin[1] in 1922. Brillouin spectroscopy has proven to be a powerful spectroscopic technique for studying the elasto-optic properties of optically transparent materials[2-6]. Brillouin studies provide accurate measurements of the sound velocity in a material. This information can then be used to determine elastic constants and structure of the material. The advent of lasers in the 1960's as monochromatic light sources and the requirement of only a small sample size has made this technique ideal for studying low temperature liquids and solids. Brillouin spectroscopy has found widespread applications ranging from the study of phase transitions in materials[7-9] to the analysis of automobile exhaust emissions.

Brillouin spectra are characterized, in frequency, by a central unshifted component, due to elastically scattered light, and upshifted and downshifted Brillouin doublets(Fig (1.1)). The intensity of the coherent, or Rayleigh, component is generally much larger

than the shifted component.

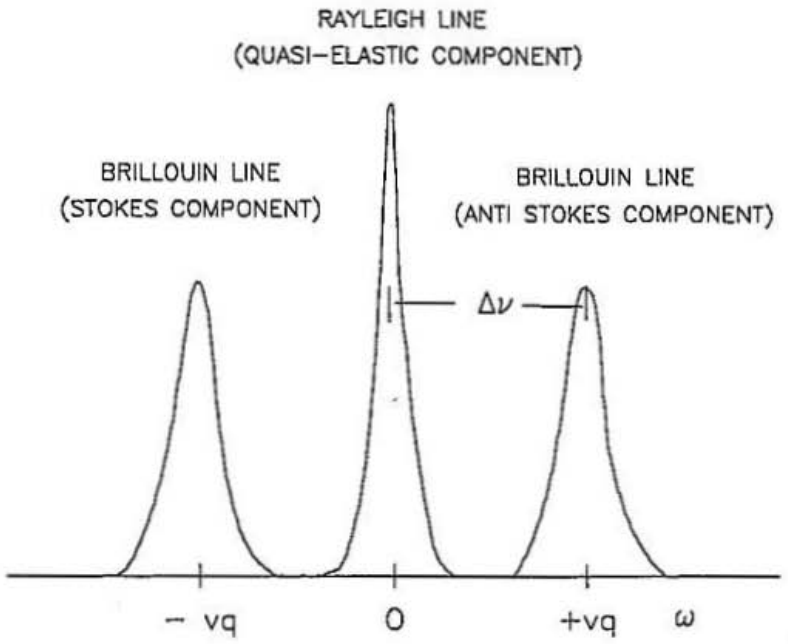

Fig. 1.1. Rayleigh–Brillouin Spectrum

Classically, Brillouin scattering can be described as the scattering of light by thermally generated sound waves, i.e. compression waves travelling through the medium. The thermal motion of molecules in a medium creates regions of compression and rarefaction resulting in localized fluctuations in the density. These variations propagate through the medium as sound waves, which, in solids, are referred to as phonons. Since these density variations produce corresponding changes in the refractive index, the sound waves may be thought of as three-dimensional diffraction gratings moving through the medium at sound velocity. Incident light waves are reflected from a grating according to

the usual Bragg diffraction condition $m\lambda=d\sin\theta$. Since the incident light is diffracted by the sound wave, i.e. a grating which is moving at the velocity of the sound, the frequency of the reflected light is shifted due to the Doppler effect. The frequency shift is equal to the frequency of the sound waves which are effective in the scattering along the particular direction of observation. The frequency shift is given by[10]

$$\Delta\nu=\pm\nu_q=\pm\frac{2nV_q}{\lambda}\sin\frac{\theta}{2} \qquad (1.1)$$

where n is the refractive index of the medium, λ the wavelength of the incident light, V_q the velocity of the sound waves in the medium in a particular direction, and θ the scattering angle. Typically, for observation of 90^0 scattering, the shift is 5-15 GHz.

Quantum mechanically[11], Brillouin scattering can be considered as the interaction between incident photons and phonons in a medium. An incident photon of frequency ν_i and wavevector $\vec{K}_i$ interacts with a phonon of frequency ν_q and wavevector $\vec{q}$, resulting in a scattered photon of frequency ν_s and wavevector $\vec{K}_s$, as shown in Fig 1.2. In this scattering process, the energy and momentum are conserved. i.e.

$$h\nu_i=h\nu_s\pm h\nu_q \qquad (1.2)$$

$$\hbar\vec{K}_i=\hbar\vec{K}_s\pm\hbar\vec{q} \qquad (1.3)$$

It is easily seen from equation (1.2) that the frequency difference between the incident photon and the scattered photon $\Delta\nu$ is equal to the phonon frequency ν_q. The momentum of the phonon $\vec{q}$ is much less than that of the photon $\vec{K}_i$, so that we can write $|\vec{K}_i|\approx|\vec{K}_s|$. From Fig 1.2, we can also write[6]

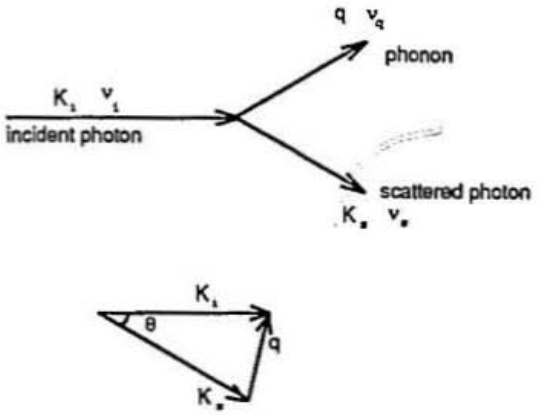

Fig 1.2 Brillouin Scattering Process

$$q=2k_i\sin\frac{\theta}{2} \qquad (1.4)$$

substituting $q=2\pi\nu_q/v_q$ and $k_i=2\pi n\nu_i/c$, where c is the light velocity, we get the Brillouin equation, as before

$$\Delta\nu=\pm\nu_q=\pm\frac{2nV_q\nu_i}{c}\sin\frac{\theta}{2} \qquad (1.5)$$

From this relation, it is clear that the light spectra will contain an upshifted and downshifted component, and that the shift will be greatest for backscattered light ($\theta=180^0$).

The Brillouin spectra observed in liquids are different from those observed in solids. According to the dynamical theory of crystals[12], the equilibrium configuration corresponds to the time averaged configuration of the crystal. Each atom executes motions about its

equilibrium position. In fluids, the atoms are not bound to equilibrium positions and are free to move over large distances. In most liquids, the major source of light scattering is from longitudinal sound waves. The Brillouin spectrum is composed of a central Rayleigh peak and two shifted peaks (Brillouin peaks) with equal and opposite splitting. In solids, both longitudinal (compressional) and transverse (shear) acoustic waves exist and have different velocities, leading to separate Brillouin scattering peaks.

1-2. Limitations of a Conventional Brillouin Scattering Apparatus

In a conventional Rayleigh-Brillouin scattering apparatus, a Fabry-Perot (FP) interferometer[11, 13] is used to obtain the frequency spectrum of the scattered light. The FP is scanned in frequency over the region containing the Brillouin spectrum. The frequency scale of the FP is calibrated using a known scatterer, such as a grating or a block of fused quartz, where the Brillouin shifts for specific scattering angles are known. Because of the weak signal, many scans must be averaged to obtain a good signal to noise ratio. Unfortunately, in some applications the use of conventional Brillouin spectroscopy has been limited by the capabilities of the interferometers employed. These limitations include limited finesse, contrast, and the absence of an internal standard for frequency calibration[14, 15].

When studying systems that exhibit complex dynamics, such as viscoelastic fluids and low temperature glasses, the technique must be capable of simultaneously measuring

large Brillouin frequency shifts and narrow linewidths with reasonable accuracy, i.e. a high finesse is required. In some materials, such as supercooled liquids, where the underlying relaxation processes occur over a broad range of time scales, the spectra must be obtained over a wide range of scattering angles and Brillouin frequencies. In such cases the parasitic broadening and strong Rayleigh peak tends to obscure the Brillouin peaks at small scattering angles, and imposes a lower limit on the range of frequencies accessible to conventional Brillouin spectroscopy.

The absence of an internal frequency standard in the interferometer limits the accuracy and precision with which Brillouin shifts and linewidths can be measured. The development of tandem interferometers[14-20] and specialized monochromators[21] with improved finesse and contrast has helped overcome some of the difficulties mentioned above, but the fundamental problems still remain. An attractive alternative invokes the coherent stimulated scattering technique which make use of the nonlinear optical properties of the medium.

1-3. Stimulated Gain Spectroscopy: Literature Review

In the early 1960's, the advent of high power pulsed lasers brought with it the discovery that these lasers produced many nonlinear effects in the medium through which the laser propagation occurred. Some examples of this are: induced defocusing, harmonic generation and the output of lower frequency light than the input laser light. This

downshifted light was recognized as being due to the Raman effect, and the process was called stimulated Raman scattering[22]. Furthermore, it was observed that under certain conditions, these laser pulses produced shock waves in the cell, filled with liquid, and in some cases would blow the windows off the cell. This was attributed to stimulated Brillouin scattering, with the subsequent generation of frequency downshifted laser light and an acoustic wave.

This idea was revived in 1977 by Owyoung[23] who observed stimulated Raman gain scattering in chlorobenzene using two continuous wave (CW) lasers. In this experiment, a tunable CW dye laser was used as a pump, to stimulate Raman gain which was then detected as a change in the HeNe probe laser intensity. When the difference frequency between the two lasers was equal to a Raman resonance in chlorobenzene, energy was transferred from the pump laser to the probe laser. The single pass gain in the experiment was about 1.0×10^{-5}. This result showed the feasibility of doing gain measurements with CW lasers. The narrow linewidth of CW lasers, compared to pulse lasers, suggested that this technique might have great promise in studying linewidths and lineshapes.

After the first observation of stimulated Brillouin scattering in the mid 1960's[24], several improvements in the frequency resolution of this technique have made coherent Brillouin spectroscopy a valuable tool for studying liquid dynamics [12, 25-28]. However, it is only in the last decade that significant improvements in frequency resolution have been made.

In 1979, Jacobson and Shen[29] first reported coherent Brillouin spectra of liquid carbon disulfide by using two lasers and a RIKES (Raman-induced kerr effect scheme) scheme[30]

in which one of the lasers was tunable. The resolution was limited by the 1 GHz linewidth of the pulsed laser. Shortly after this, in 1983, She [31,32] et al obtained stimulated Rayleigh-Brillouin (BG) gain spectra of some pure gases and gas mixtures using a single-mode pulsed laser. The frequency resolution was again limited by the linewidth of the pulsed lasers used. In 1987, they used a CW frequency-stabilized laser to obtain the BG spectrum of SF_6, with a resolution of about 4 MHz[33]. The resulting linewidth measurements agreed very well with the theoretical predictions. Included were the first measurements of forward scattering at small angles. A high-resolution Brillouin study in fused silica, glasses and crystals using pulsed lasers was reported by Faris et al[34-36]. It should be noted that in BG spectroscopy, the Rayleigh line present in conventional Brillouin spectra, is not present, allowing for very small angle scattering measurements, which are normally obscured by this peak.

More recently, since 1991, a great deal of work has been done on CS_2 and glycerol in the liquid state by Grubbs and MacPhail[37-42]. This work has clearly shown that BG spectroscopy with CW lasers is possible and can provide very accurate Brillouin measurements of the liquid state, including accurate lineshape measurements.

In this thesis we will describe a CW Brillouin gain spectrometer which we have constructed. The spectrometer utilizes a Coherent 699-29 Dye laser as a pump laser and a stabilized HeNe laser as a probe laser. The results of measurements on liquid CS_2 and CCl_4 will be presented.

In Chapter 2, the theory of stimulated Brillouin scattering (SBS) will be presented. Chapter 3 will be a detailed description of the BG spectrometer. A great deal of time on

this project was spent constructing and improving this apparatus. Several improvements to the apparatus and the experimental technique will also be presented. Chapter 4 is a presentation of the results from liquids CS_2 and CCl_4. A comparison of these results with theory will be given. In Chapter 5, a summary of our work along with conclusions is given.

CHAPTER 2.

THEORY OF STIMULATED BRILLOUIN GAIN SPECTROSCOPY

2-1. Stimulated Brillouin Scattering.

The phenomenon of stimulated Brillouin scattering[24, 43] occurs when the acoustic wave that scatters the optical beam is produced by the optical beam itself.

When an intense laser beam of frequency ω_l passes through a medium, a coherent acoustic wave at a frequency ω_q is produced within the medium and at the same time an optical beam is generated.The optical frequency, according to energy conservation, is ω_l - ω_q. Both the acoustic and scattered optical beams are emitted along specific directions. The directions can be determined from momentum conservation where the wavevectors satisfy the condition $\vec{K}_l=\vec{K}_q+\vec{K}_s$.

Stimulated Brillouin scattering occurs only when the incident light intensity approaches a well-defined threshold value[44]. This threshold value is typically 10^9 W/cm^2 for most gases, liquids, and solids[45].

2-2. Brillouin Gain Spectroscopy

In a stimulated Brillouin scattering experiment, a strong laser beam, with frequency and wavevector (ω_2, k_2), and a weaker probe laser beam, with frequency and wavevector(ω_1, k_1), are loosely focused and overlapped at an angle θ in a sample cell. The two beams interact in the sample and, through electrostriction, the medium produces an acoustic wave whose frequency and wavevector are $\Omega=\omega_2-\omega_1$ and $\vec{K}=\vec{K}_2-\vec{K}_1$, respectively. When the difference frequency Ω is equal to the Brillouin frequency, energy will be transferred between the higher frequency beam and the lower frequency beam through interaction with the acoustic wave. By tuning the pump beam frequency and simultaneously monitoring the probe intensity, a stimulated Brillouin gain spectrum is generated, such that the gain (or loss) in the probe power is plotted versus Ω. The Brillouin shift is still expressed by equation (1.5), but now θ is the crossing angle between the pump and probe laser beams.

2-3. Expression of Brillouin Gain[31, 44, 46]

Consider a finite box of volume V containing N molecules . The number density fluctuation at point $\vec{r}$ at time t is $\delta\rho(\vec{r},t)$. This density fluctuation may be written as

function of wavevector $\vec{K}_j$ and angular frequencies Ω_j, according to the Fourier transform:

$$\delta\rho(\vec{K}_j,t)=\int\delta\rho(\vec{r},t)e^{-i\vec{K}_j\cdot\vec{r}}d^3\vec{r} \qquad (2.1)$$

$$\textit{where} \quad \delta\rho(\vec{r},t)=\frac{1}{V}\sum_j\delta\rho(\vec{K}_j)e^{-i\Omega_j t}e^{i\vec{K}_j\cdot\vec{r}} \qquad (2.2)$$

and $\delta\rho(\vec{K}_j,t)=\delta\rho(\vec{K}_j)e^{-i\Omega_j t}$.

For a given $\vec{K}$, the autocorrelation function of $\delta\rho(\vec{K})$ may be expressed in terms of its power spectral density $\Phi(\vec{K},\Omega)$ as

$$<\delta\rho(\vec{K},t)\delta^*\rho(\vec{K},0)>=\int e^{-i\Omega t}\Phi(\vec{K},\Omega)d\Omega \qquad (2.3)$$

where < > denotes an ensemble average. The normalized spectral density per molecule

$$S(\vec{K},\Omega)=\frac{1}{N}\Phi(\vec{K},\Omega) \qquad (2.4)$$

is the space-time Fourier transformation of the Van Hove's space-time correlation function G(r,t)[47].

Assuming two electric fields are in the form of plane waves travelling in an arbitrary direction.

$$\vec{E}_1(\vec{r},t)=\frac{1}{2}\vec{E}_1e^{i(\vec{K}_1\cdot\vec{r}-\omega_1 t)}+c.c \qquad (2.5)$$

$$\vec{E}_2(\vec{r},t)=\frac{1}{2}\vec{E}_2e^{i(\vec{K}_2\cdot\vec{r}-\omega_2 t)}+c.c \qquad (2.6)$$

In a light scattering experiment, the density fluctuation is excited by the pump field $\vec{E}_2(\vec{r},t)$. In coherent gain spectroscopy, the excited density fluctuation is probed by the probe field $\vec{E}_1(\vec{r},t)$. The pump and probe fields select a normal mode with a particular $(\vec{K},\Omega)$, which satisfies momentum and energy conservation, i.e. $\vec{K}=\vec{K}_1-\vec{K}_2$ *and* $\Omega=\omega_1-\omega_2$. In this manner, the intensity of the probe beam is modified (stimulated gain or loss) by

the density fluctuation $\delta\rho(\vec{K})e^{-i\Omega t}$. The electric field acting on the molecule is

$$\begin{aligned}\vec{E}(\vec{r},t) &= \vec{E}_1(\vec{r},t)+\vec{E}_2(\vec{r},t) \\ &= \frac{1}{2}[\vec{E}_1 e^{i(\vec{k}_1\vec{r}-\omega_1 t)}+\vec{E}_2 e^{i(\vec{k}_2\vec{r}-\omega_2 t)}+c.c] \ . \end{aligned} \qquad (2.7)$$

The density change due to this field will modify the permittivity ε of the medium. As a result, the molecules gain potential energy from the fields:

$$\begin{aligned}\Delta W &= \frac{1}{2}\int \delta\varepsilon |\vec{E}(\vec{r},t)|^2 d^3\vec{r} \\ &= \frac{1}{2}\int (\frac{\partial\varepsilon}{\partial\rho})_0 \delta\rho(\vec{r},t)|\vec{E}(\vec{r},t)|^2 d^3\vec{r} \ . \end{aligned} \qquad (2.8)$$

Substituting eqs (2.2) and (2.7) into (2.8), we obtain the energy of the excited normal mode as

$$\Delta W = \frac{1}{4}(\frac{\partial\varepsilon}{\partial\rho})_0 \vec{E}_2^{\,*}\cdot\vec{E}_1\delta\rho(\vec{K}) \qquad (2.9)$$

Equation (2.9) suggests the existence of a force

$$f_{\vec{K}} = -\frac{d(\Delta W)}{d(\delta\rho)} = -\frac{1}{4}(\frac{\partial\varepsilon}{\partial\rho})_0 \vec{E}_2^{\,*}\cdot\vec{E}_1 \qquad (2.10)$$

which induces the density fluctuation

$$\delta\rho(\vec{K}) = R(\Omega)f_{\vec{K}} \ , \qquad (2.11)$$

where R(Ω) is the response function depending on the dynamics of the medium. To ultimately relate to the gain coefficient, the amplitude of the associated third-order polarization is usually written[44] , for one normal mode, as

$$
\begin{aligned}
P^{(3)} &= \delta \epsilon E_2 \\
&= (\frac{\partial \epsilon}{\partial \rho})_0 \delta \rho(\vec{r}) E_2 \\
&= (\frac{\partial \epsilon}{\partial \rho})_0 \frac{\delta \rho(\vec{K})}{V} E_2 \\
&= -\frac{1}{4V} [\frac{\partial \epsilon}{\partial \rho}]_0^2 R(\Omega) |E_2|^2 E_1 \\
&\equiv \chi^{(3)}(\omega_1) |E_2|^2 E_1 \quad . \qquad (2.12)
\end{aligned}
$$

Solving the wave equation:

$$
\nabla^2 \vec{E}_1(\vec{r},t) = \mu \epsilon \frac{\partial^2}{\partial t^2} \vec{E}_1(\vec{r},t) + \mu \frac{\partial^2}{\partial t^2} \vec{P}^{(3)} \qquad (2.13)
$$

in the steady state, under the slowly varying wave approximation, the Stokes probe field grows according to

$$
\frac{dE_1}{dz} = i \frac{\omega_1}{2c\epsilon_0} \chi E_1, \qquad \chi = \chi^{(3)} |E_2|^2 \quad . \qquad (2.14)
$$

The gain coefficient is

$$
g \equiv \frac{1}{I} \frac{\partial I}{\partial z} \quad where \quad I \equiv \frac{c\epsilon}{2n} |E|^2 \quad .
$$

Solving equation (2.12) and (2.14), we obtain the gain coefficient for the probe beam:

$$
g(\omega_1) = -\frac{2\omega_1}{(c\epsilon_0)^2} (I_m \chi^{(3)}) I_2 \qquad (2.15a)
$$

$$
= -\frac{2\omega_1}{(c\epsilon_0)^2} [-\frac{1}{4V} (\frac{\partial \epsilon}{\partial \rho})_0^2 I_m R(\Omega)] I_2 \qquad (2.15b)
$$

where I_2 is the intensity of the pump beam. Equation (2.15a) indicates that the gain coefficient is proportional to the third-order nonlinear susceptibility.

In equation (2.15b), the imaginary part of the response function R (Ω) relates to the spectral density function by the fluctuation dissipation theorem, as

$$\frac{k_B T}{\pi \Omega} I_m R(\Omega) = \Phi(\vec{K},\Omega) = NS(\vec{K},\Omega) \quad . \qquad (2.16)$$

Also, in equation (2.15b), $(\frac{\partial e}{\partial \rho})_0$ is the molecular polarizability α. It can be related to the Rayleigh cross section by electromagnetic theory as

$$(\frac{\partial e}{\partial \rho})_0^2 = \alpha^2 = \frac{(4\pi e_0)^2}{k_1^4} \frac{d\sigma}{d\Omega} \quad , \qquad (2.17)$$

where $\frac{d\sigma}{d\Omega}$ is the differential Rayleigh cross section. Substituting eqs (2.16) and (2.17) into eqs (2.15), the Brillouin gain coefficient can be expressed as :

$$g(\omega_1) = \frac{8\pi^3 c^2}{\omega_1^3} \frac{\rho_0}{k_B T} [\Omega S(\vec{K},\Omega)] \frac{d\sigma}{d\Omega} I_2 \qquad (2.18)$$

Usually, cross-sectional intensity profile of a laser beam is Gaussian, and the total gain of the interaction can be shown to be[31]:

$$G = \eta_c \frac{4\pi^3 c \omega_2}{\omega_1^3} \frac{\rho_0}{k_B T} [\Omega S(\vec{K},\Omega)] \frac{d\sigma}{d\Omega} P_2 \qquad (2.19)$$

where η_c is the crossing efficiency of the two beams and P_2 is the power of the pump beam. Equations (2.18) and (2.19) are the expressions for the gain coefficient and total gain in the steady state respectively. They are linearly proportional to the pump intensity or power.

2-4. Advantages of a Stimulated Brillouin Gain Spectroscopy Apparatus

Stimulated Brillouin gain spectroscopy has all of the usual advantages associated with coherent spectroscopies, such as, high signal-to-noise ratio and excellent

discrimination from stray light and fluorescence backgrounds. This technique also offers several advantages over conventional interferometric Brillouin scattering techniques. In eq (2.19) , the $\Omega=\omega_2-\omega_1$ factor appearing in the gain expression goes to zero as $\omega_2\rightarrow\omega_1$ thereby suppressing the Rayleigh peak in the spectrum. This is particularly important for small angle scattering, where the Brillouin shift is small and Brillouin peaks may be obscured by the Rayleigh peak. In addition, the frequency resolution in BGS is limited only by the linewidths of the lasers (typically < 4MHz), so that high resolution can be obtained by employing narrow linewidth continuous-wave (CW) lasers. In addition, the difference between the frequencies of the pump and probe beams can be determined very accurately, allowing for a highly accurate determination of the frequency of the peaks in the gain spectrum and thus accurate measurements of spectral shifts and linewidths. The available spectral range is only restricted by the tuning range of the pump laser. In contrast to conventional Brillouin spectroscopy, this technique permits measurement of large Brillouin shifts and narrow linewidths, something which is difficult to do with a Fabry Perot interferometer. Finally, the scattering wavevector $\vec{K}$ is precisely defined by the crossing angle θ of the pump and probe laser beams.

CHAPTER 3.

EXPERIMENTAL SETUP AND TECHNIQUE

3-1. Brillouin Gain Spectrometer

The experimental setup for Brillouin gain spectroscopy is shown in figure 3.1. The pump and probe beams with parallel polarizations were focused and overlapped in the sample cell by a pair of lenses (L_3,f=20 cm and L_4,f=40 cm) using a backscattering geometry. The pump beam was provided by a frequency stabilized, scanning ring dye laser (Coherent CR 699-29), which is pumped with the multi-line output of a Coherent Innova 90-6 argon ion laser. In the experiment, the pump laser beam power was typically 120-150 mW at 633 nm using Kiton Red dye. The jitter in the pump laser frequency was previously measured to be less than 2 MHz. The probe beam was provided by a polarized single-frequency (632.8 nm) stabilized HeNe laser (Spectra-Physics Model 117) with an output power of 1.7 mW. The wavemeter, computer and software of the Coherent CR 699-29 were used to record the probe gain (or loss) as a function of pump frequency. In order to enhance the signal-to-noise ratio of the Brillouin gain signal, which is typically

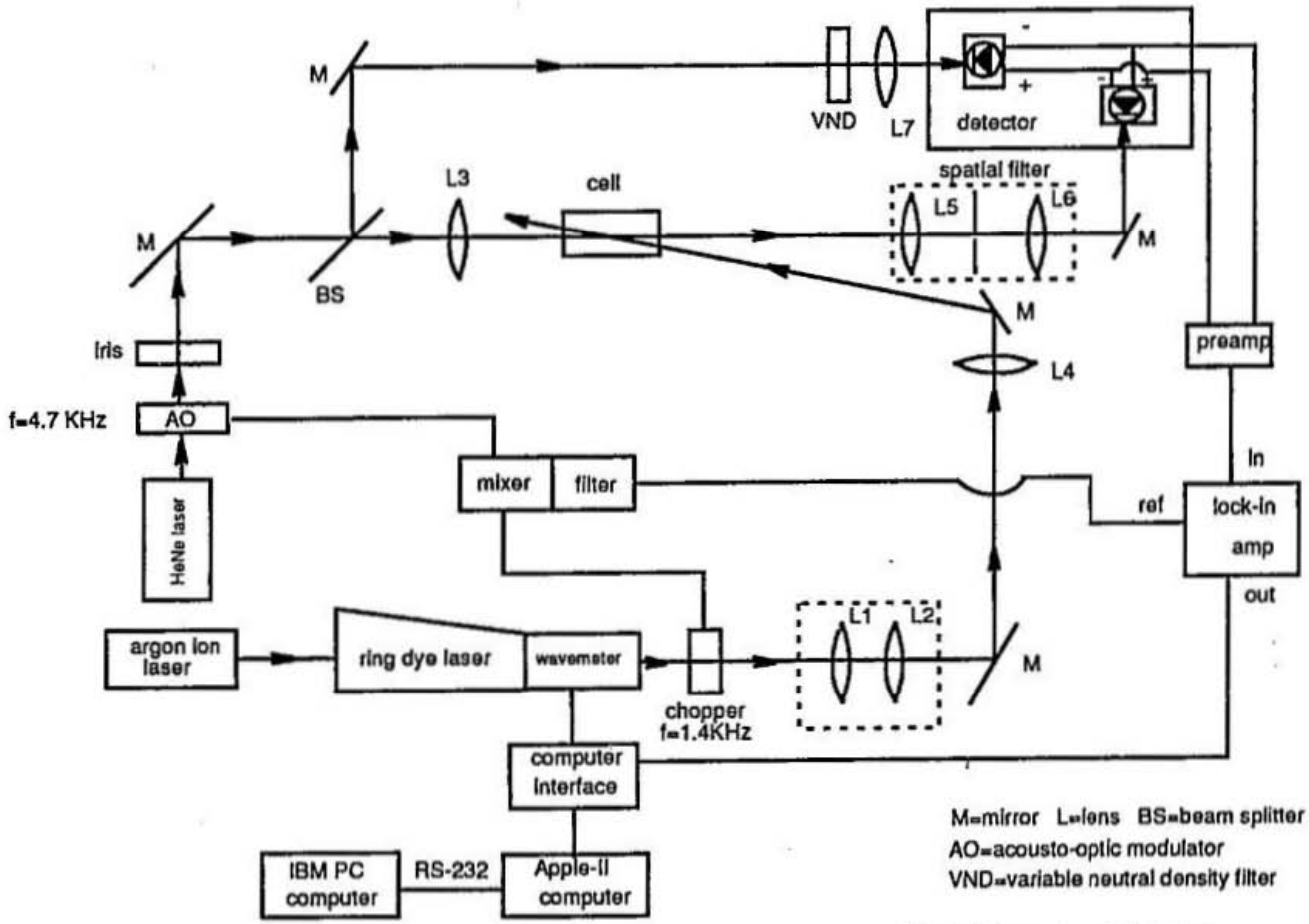

Fig.3.1 Experimental Setup

1 part in 10^6 of the probe intensity , a double modulation technique and a balanced detection scheme were used.

3-2. Coherent Radiation 699-29 Autoscan Ring Dye Laser System [48-51]

Figure 3.2 shows the configuration of the CR 699-29 autoscan ring dye laser system. This system is controlled by an Apple II computer and can scan in frequency over a range of up to 10 THz (10^4 GHz) with better than 4 MHz resolution. It can also provide an absolute wavelength readout to an accuracy < 4×10^{-7} nm, digitize and store data under active computer control, and present the data as seamless spectra, normalized to the dye laser power.

The width of the gain profile of the laser dye, in this case Kiton Red, is about 30 nm. Single frequency operation is obtained by the use of several intracavity elements. A 3-plate birefringent filter (BRF) and a pair of etalons (thick etalon and thin etalon) form the tunable filter stack, which selects a single frequency. These optical elements have free spectral ranges of 1680 GHz, 10 GHz and 225 GHz respectively, producing a final laser linewidth of about 2 MHz. In practice, due to acoustic noise, etc., the longterm linewidth is slightly larger than this (< 4 MHz).

The operating wavelength of the dye laser was determined by a built in wavemeter. This wavemeter consists of a high resolution vernier etalon (VET) and a low resolution optical activity monochromator (OAM). The OAM consists of two different lengths of

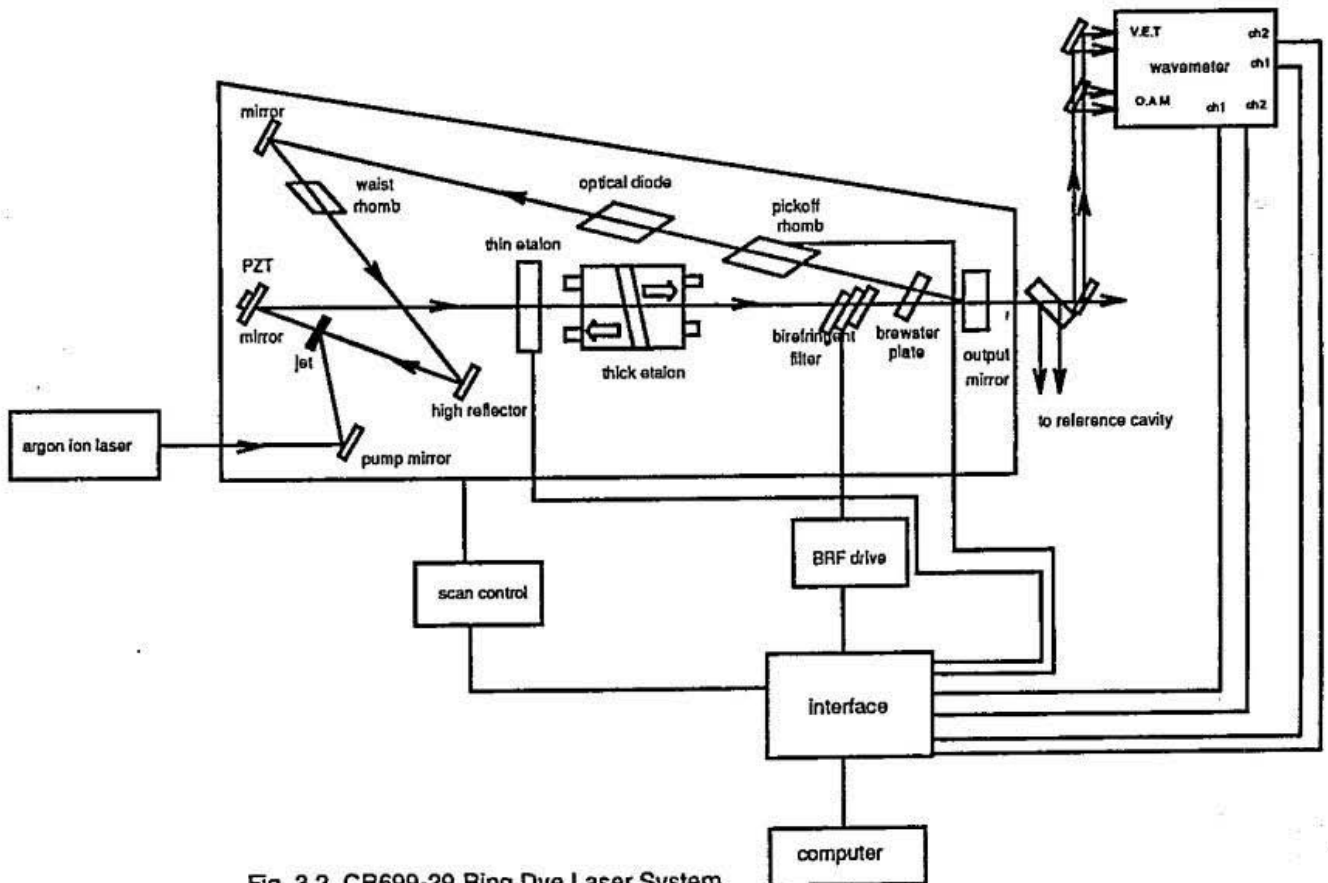

Fig. 3.2. CR699-29 Ring Dye Laser System

optically active quartz. The laser beam is split into two parts and then passed through these crystals. The resulting light is analyzed for polarization, and a coarse wavelength is determined from a look up table stored in the computer. The VET consists of two temperature stabilized etalons, of slightly different length. In a given etalon order, the transmission maxima of the two etalons have a unique relationship, very similar to the vernier scale principle. To determine the laser wavelength, the laser is scanned over a short 10 GHz region. A coarse wavelength reading is determined from the OAM, which then uniquely determines the VET order. Once the VET order is known, the computer calculates the wavelength to better than 4×10^{-7} nm.

Because of alignment errors, as the light passes through the wavemeter etalons, the frequencies measured by the wavemeter are often shifted slightly from the correct values. The shift can be determined, and corrected for, by periodically measuring the absorption spectrum of low pressure I_2 vapour and then comparing with the known spectrum[52]. The setup for this calibration is shown in Fig 3.3. The wavemeter was then corrected by this value. This correction is significant, as a typical signal scan is only 0.25 cm^{-1}, and an error in calibration could mean missing the BG signal altogether. Figure 3.4 shows a typical set of I_2 scan data, in which the wavemeter was found to be shifted to lower frequency by 0.2358 cm^{-1}.

It is important to note that the wavemeter had to be recalibrated each time the laser was more than slightly adjusted. Any large adjustments of the laser mirrors means that the light will travel through the wavemeter etalons at a slightly different angle, and hence, the wavemeter will read differently. The sensitivity of this laser to temperature changes

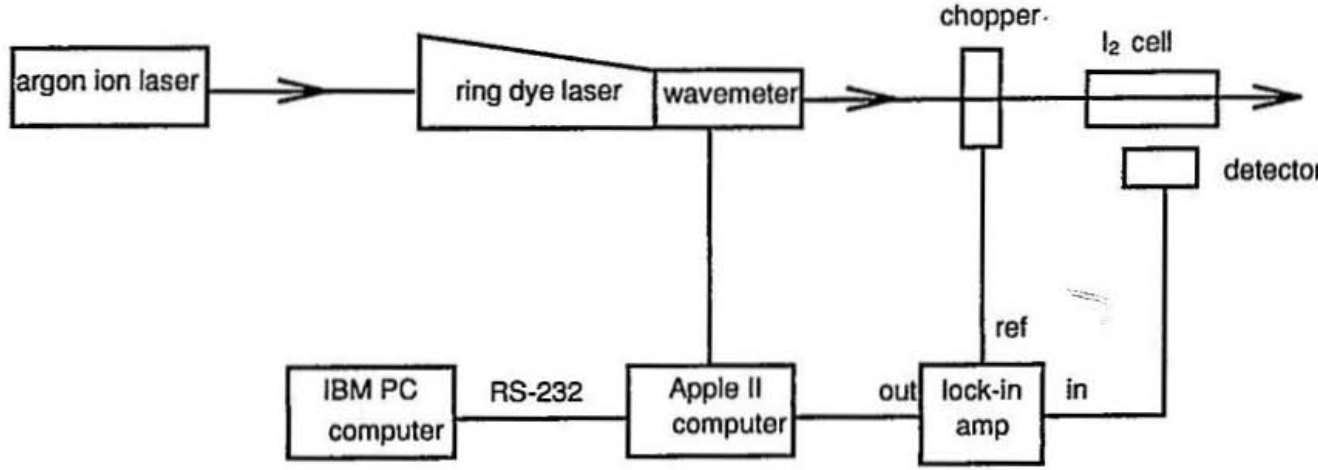

Fig. 3.3 Scheme for Laser Calibration

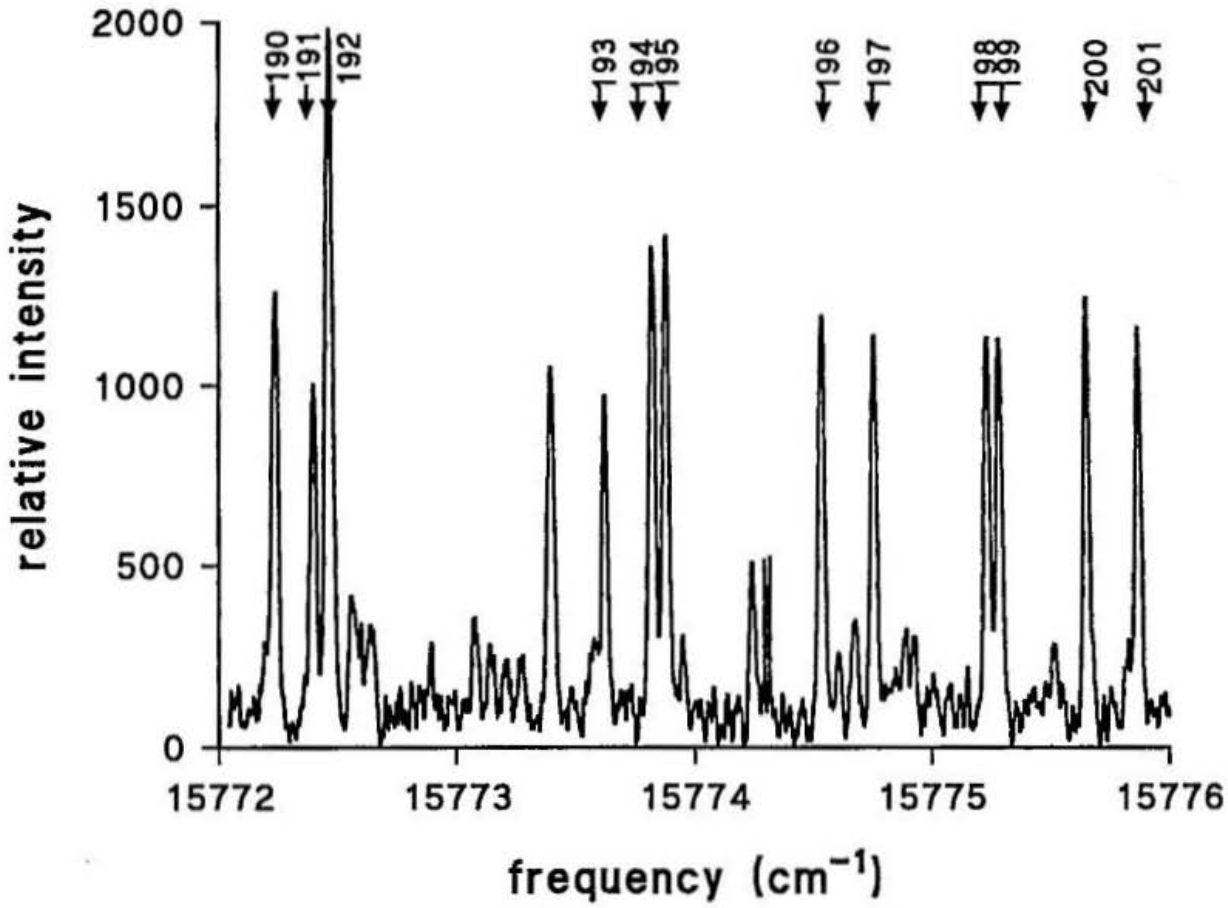

Fig 3.4 I_2 Absorption Spectrum

Table 3.1. Calibration of the laser shift

line	measured frequency (cm^{-1})	standard frequency (cm^{-1})	shift (cm^{-1})
190	15772.2393	15772.4773	0.2380
191	15772.4000	15772.6364	0.2364
192	15772.4656	15772.6976	0.2320
193	15773.6229	15773.8571	0.2342
194	15773.8234	15774.0609	0.2375
195	15773.8815	15774.1152	0.2337
196	15774.5364	15774.7703	0.2339
197	15774.7560	15774.9918	0.2358
198	15775.2313	15775.4662	0.2349
199	15775.2827	15775.5166	0.2339
200	15775.6487	15775.8867	0.2380
201	15775.8679	15776.1096	0.2417
mean value	N/A	N/A	0.2358

means that a great number of these calibrations must be carried out. It is almost a full-time job to keep the CR 699-29 aligned properly and calibrated.

3-3. Noise-reduction Schemes

Since the magnitude of the Brillouin gain signal is very small, at best about 1 part in 10^5 of the probe beam intensity, several noise-reduction schemes were employed to enhance the signal-to-noise ratio. A double modulation scheme[53], similar to that used in intermodulated fluorescence spectroscopy, is used to reject noise which is not at the signal modulation frequency. A major source of noise in this experiment is power amplitude fluctuation of the probe laser. To further enhance the signal to noise ratio, a balanced detection scheme[54] was used for the probe laser beam, effectively reducing such noise.

3-3-1. Double Modulation Technique

We have employed a double modulation technique, in which the pump and probe beams are each modulated at different frequencies and the gain signal is detected synchronously using a lock-in amplifier tuned to the difference frequency. This allows for rejection of spurious signals from stray pump reflections at the detector.

In our SBG experiment, the pump beam was modulated at 1.4 KHz by a mechanical chopper (Chopper OC 4000), and the probe beam at 4.7 KHz by an acousto-optic (AO)

modulator. Initially, we tried modulating the pump beam at 19.2 KHz by an AO modulator while the probe beam was mechanically chopped at 2 KHz. The gain signal was detected synchronously at 17.2 KHz by a lock-in amplifier (Stanford Research system SR510) with a input filter Q of 10. Experimentally it was determined that the pump and probe modulation frequencies were too close, within the bandwidth of the filter, and that leakage from the pump at 19.2 KHz was swamping the difference frequency signal at 17.2 KHz. To make effective use of the Q=10 lock-in filter, the pump modulation frequency was reduced to 4.7 KHz and the probe modulation to 1.4 KHz (as noted above), so that the difference frequency was 3.3 KHz. The reference signals from the chopper and AO modulator were electronically mixed in a diode mixer (Watkins-Johnson (WJ-M1)), amplified and filtered to remove harmonics, to produce a reference signal at the difference frequency (3.3 KHz) for use in lock-in detection. Figure 3.5 shows the electronic schematic for this circuit. The TTL(0-5V) signal from the mechanical chopper was level shifted and transformed to a ±2.5V sine wave by the upper amplifier stage. This sine wave was then fed into one input of the mixer. The output of the mixer contained many harmonics of f1 and f2, as well as the difference frequency. Consequently, the last three stages are bandpass filters with a center frequency of 3.3 KHz and a quality factor of 15. The output of the circuit is a good clean 1V p-p sine wave with a frequency of 3.3 KHz.

The electronics for the experiment were then tested by observing linear and doppler-free fluorescence from low pressure I_2 vapour[55]. The doppler-free fluorescence signal is generated by I_2 molecules which absorb both laser beams simultaneously, that is, the

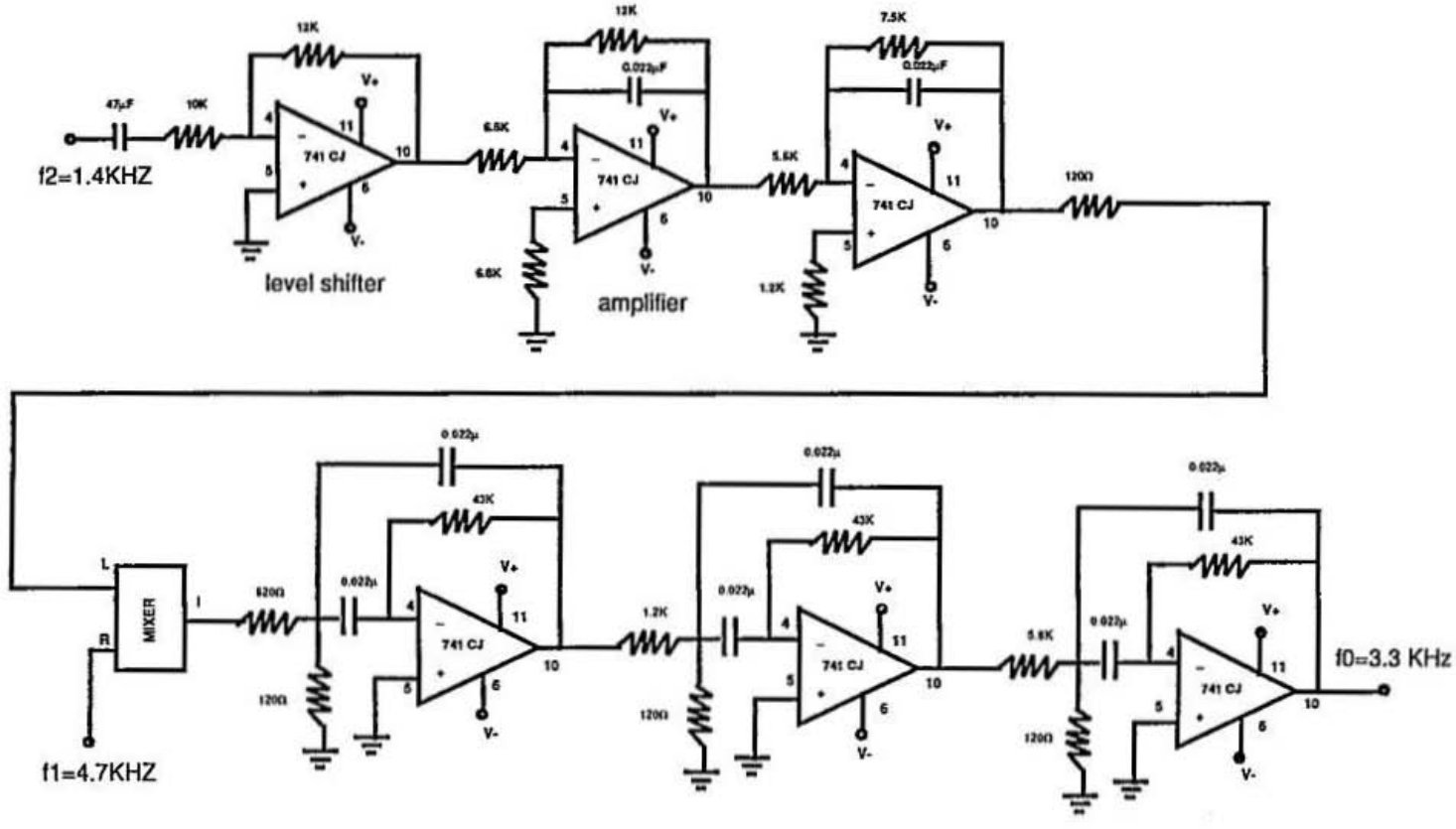

Fig.3.5 Electronic Circuit of the Filter

molecules which are moving perpendicular to both beams. Detection of the doppler-free fluorescence signal requires that the fluorescence signal be detected at the difference frequency, and hence serves as a good test of our difference frequency circuitry. The experimental setup is shown in fig 3.6. The dye laser beam was split into two parts, modulated at two frequencies f1 and f2, and overlapped at the centre of a cell containing I_2 vapour. A photodiode at the side of the cell monitored the fluorescence as the dye laser was tuned over a 5 GHz range. Lock-in detection at frequency f1 or f2 yielded the linear fluorescence spectrum (Fig 3.7a), while detection at the difference frequency produced the doppler-free intermodulated fluorescence spectrum (Fig 3.7b). The advantage of the difference frequency detection is obvious. The fact that the doppler-free spectra can be detected verified that the electronics circuit, we built, works very well.

3-3-2. Balanced Detection Scheme

The Brillouin peak gain is typically 10^{-5} of the intensity of the probe beam. Any amplitude fluctuations in the probe beam can obscure the gain signal. In order to suppress this noise, a balanced detection scheme was used (see figure 3.1). The HeNe probe beam is split into a signal beam and a reference beam by a 50/50 beam splitter . The signal beam goes through the sample cell to the silicon photodiode (Silicon Detector Corp. SD-200-12-12-241). The reference beam traverses a similar distance and is focused onto a matched photodiode. The two photovoltaic diodes are isolated from their cases and are

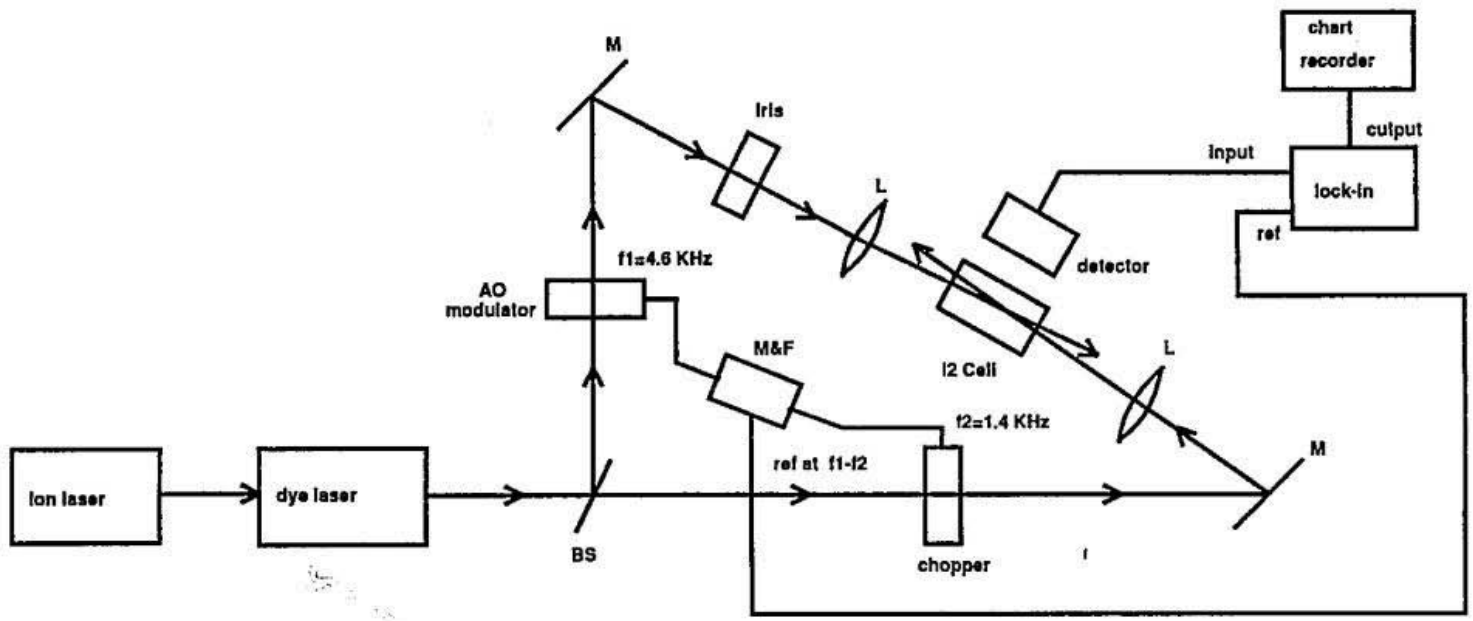

AO=Acousto-optic, M&F=Mixer and Filter

M=Mirror, L=Lens, BS=Beamsplitter

Fig.3.6 Setup for Fluorescence Spectra

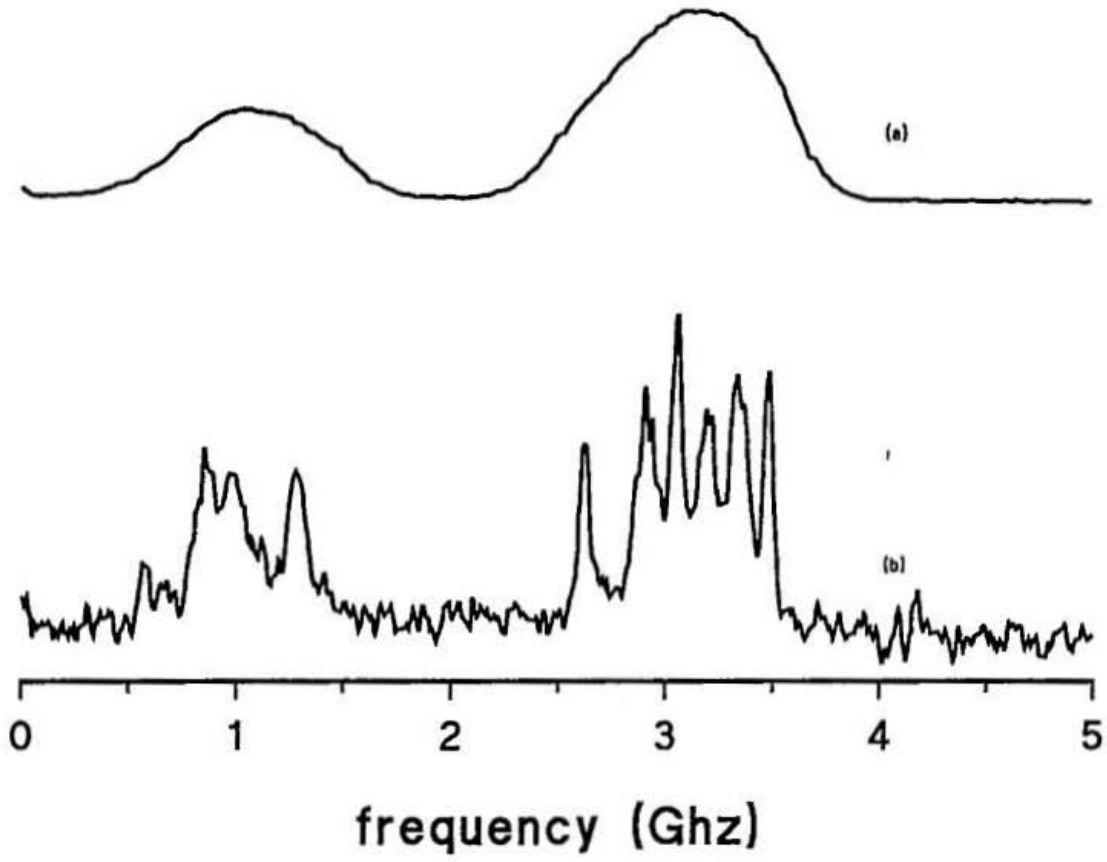

Fig.3.7 (a) I_2 Fluorescence Spectrum as Function of Frequency (b)Intermodulated Fluorescence Spectrum

connected in a push-pull configuration.

In the push-pull arrangement the anode of one photodiode is connected to the cathode of the second photodiode and vice versa. The output is measured across either diode. If light falling on both photodiodes is the same, then the output from the pair will be zero. The diodes in effect act as a differential amplifier. The output of the diode pair is used as input to a high gain current preamplifier. The output of the preamplifier is fed into a lock-in amplifier (Princeton Applied Research model 124A). By using a variable neutral density filter in the reference beam to balance the signals on the two photodiodes, the current into the input of current amplifier is zeroed. This has the effect that much of the noise due to the probe beam amplitude fluctuations is cancelled out.

A key part of this setup is that the two photodiodes are connected in a push-pull configuration with very short leads. Earlier in this work we attempted using separate photodetectors /preamps in the signal beam and reference beam. These were respectively fed into the differential input of the lock-in amplifier channel (Stanford Research System SR510). Due to cable capacitance, the phases of the two signals from the photodetectors were slightly different. We would invariably see a large noise pulses in the output of the differential amplifier. Comparing these two schemes, the advantage of the push-pull configuration is that much of the large background noise can be nulled before amplification and the gain on the preamp can be turned up higher without saturating it.

3-3-3. Additional Refinements to Our Noise Reduction Scheme

Our initial experimental setup incorporated both the balanced detection scheme and the double modulation technique. We were however unable to observe any BG signal. It was suspected that because of the high collinearity of the pump-probe beams some pump light was being reflected either into the photodiodes, or directly into the HeNe probe laser. Scattered pump light entering unequally into the photodiodes would not be cancelled out by the balanced detection scheme, and would, to a certain degree, contribute amplitude noise to the difference frequency signal. In order to prevent the reflections of the pump beam from entering the detector, a spatial filter using a 20 cm lens and a 200 μm pinhole was used in the signal beam path. It effectively reduced the noise due to the stray pump beam reflections.

Light entering the probe laser is a bigger concern, since it could cause the probe laser power to fluctuate, as the electronics try to stabilize the light intensity. When the probe laser amplitude varies, the signal from the photodiodes becomes unbalanced. This unbalanced signal contributes a large varying synchronous background which is much bigger than the BG signal. A great deal of care was taken to ensure that very little pump laser light was incident on the entrance aperture of the HeNe laser. There was of course a tradeoff here. In backward scattering, as the angle gets bigger, the BG signal gets larger and the light scattered into the HeNe laser increases.

At this point in our investigation, we had still not observed a BG signal. Because of

the long pathlengths traversed by the probe beam(about 2m), the amplitude fluctuations from the airborne dust particles could contribute substantial noise that would not be cancelled by the balanced detection scheme. Upon confirming that the rest of the experimental setup was functioning properly, and after many fruitless hours of searching for a signal , we placed the entire probe beam-sample cell-detector setup inside a covered plexiglass box[41]. Almost immediately we saw our first gain signal in CS_2(fig 3.8).

3-4. Procedure for Overlapping The Pump and Probe Beams

In our experimental setup, a great deal of effort was made to maximize the overlap of the pump and probe beams. The objective was to bring both beams to a common focus with matching beam waists. From equation (2.19), the Brillouin gain signal is proportional to the beam crossing efficiency η_c. A value of η_c=0 indicates that there is no overlap, whereas η_c=1 indicates complete overlap. In the experiment, in order to maximize the beam overlap, we first calculated the focal position and focal diameter of the probe beam inside the cell and then using a simple telescope (L_1 and L_2 in Fig 3.1) matched the diameter of the pump and probe beams at their mutual focus. The focal point for the pump beam was set by moving lens L_4. To maximize the overlap of the pump and probe beams it was first necessary to determine the characteristics of each of the Gaussian beams produced by the lasers. To do this, a small pinhole on an xy mount was placed between the laser and a large aperture power meter. By moving the pinhole through the

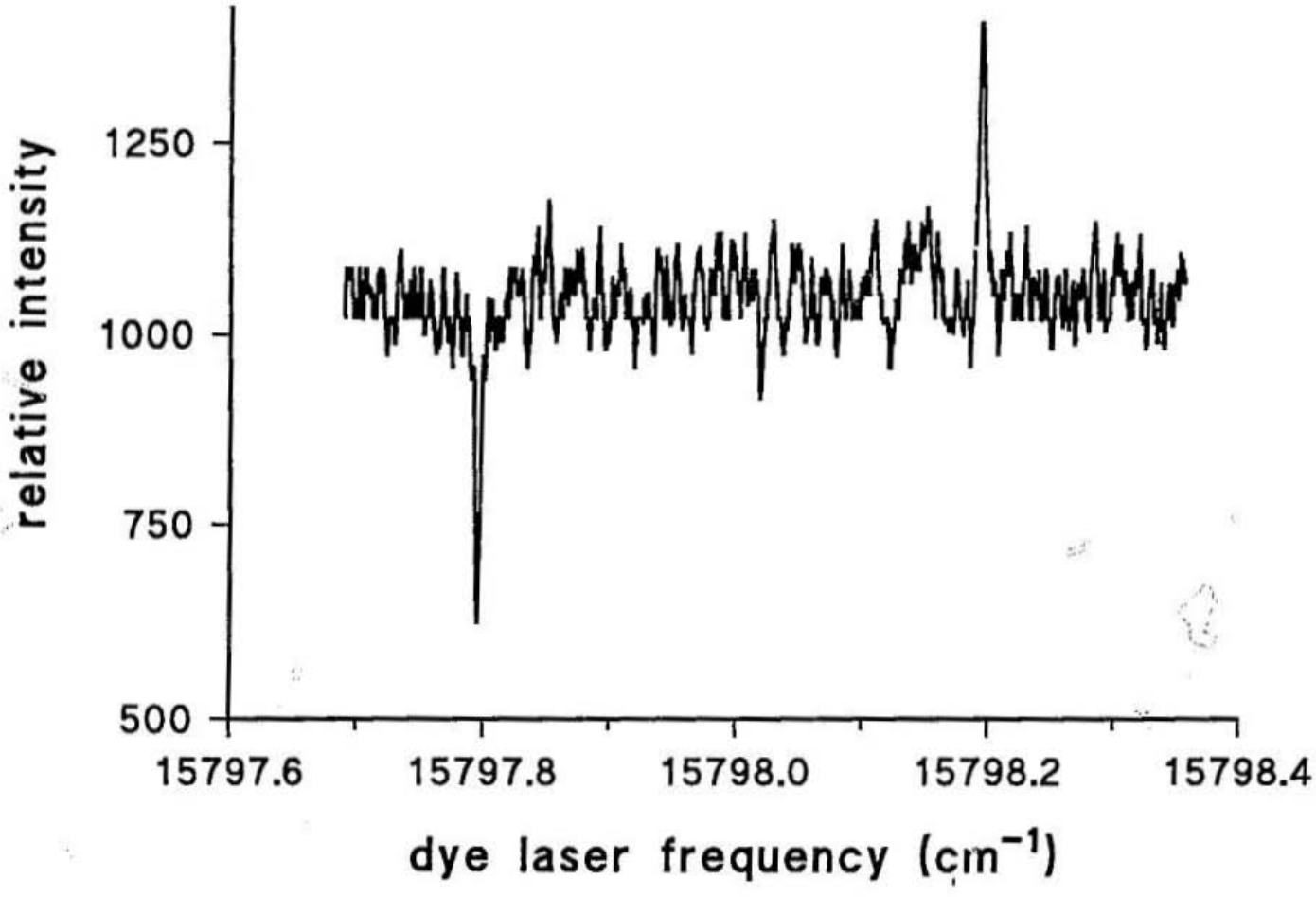

fig3.8 First Brillouin Gain Signal of CS_2

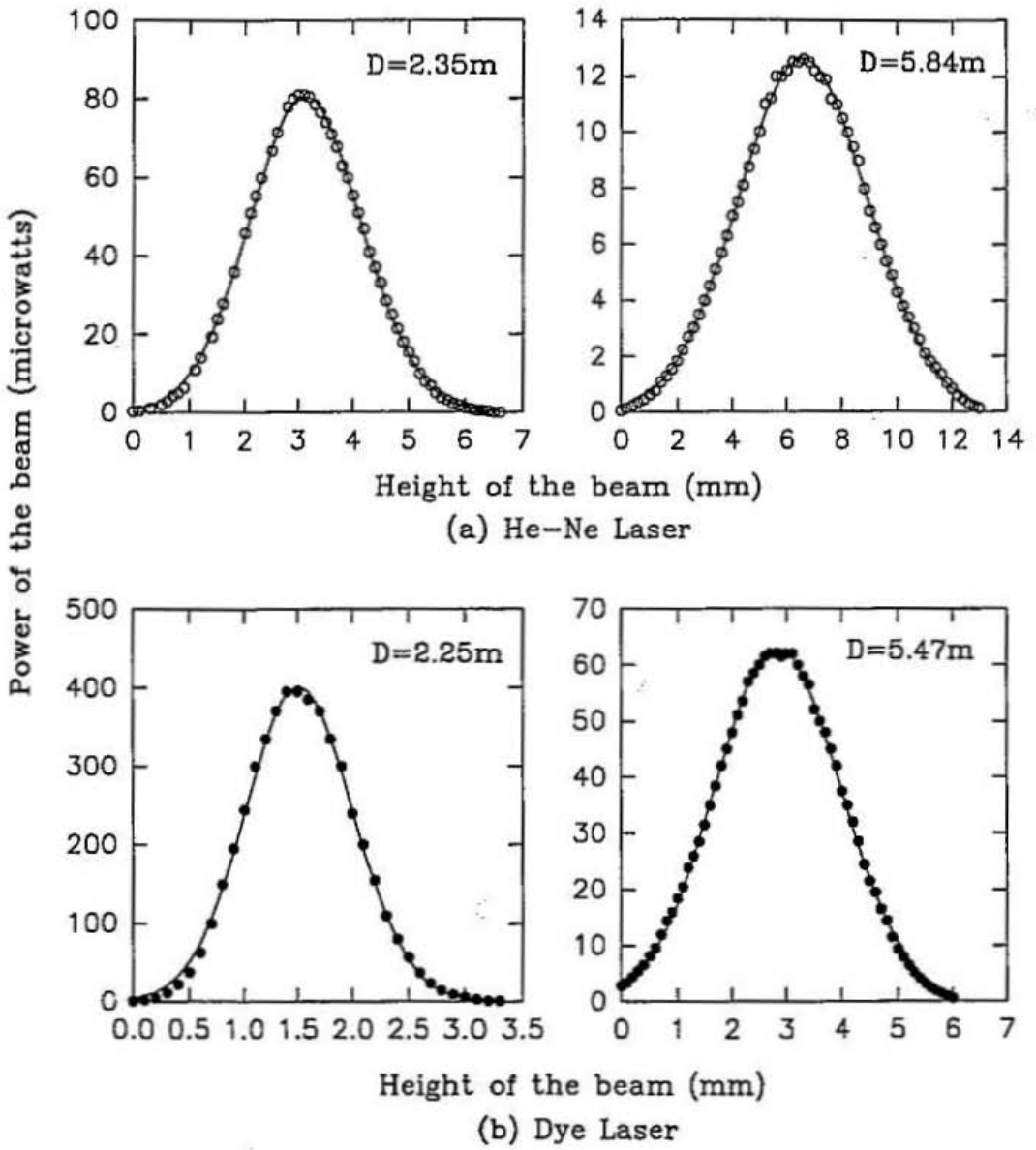

Fig 3.9 Gaussian Profiles of Laser Beams

laser beam, the radial intensity distribution of each of the laser beams was determined. Typical profiles, at two distances, are shown in Fig 3.9. The solid lines correspond to fits of Gaussian profiles to the experimental data. D is the distance between the measured plane and the laser output mirror and h is the distance between the measured point to the edge of the laser beam in the measuring plane(Fig 3.10). The Gaussian fitting results

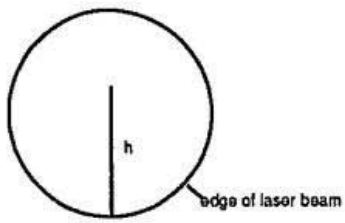

Fig 3.10 Laser Beam Cross Section

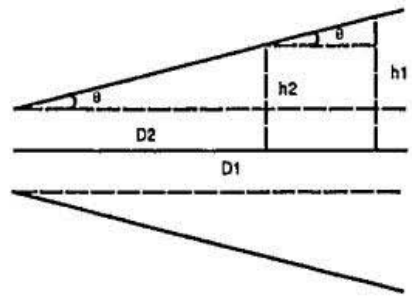

$$\text{divergence } \theta = \frac{h1-h2}{D1-D2}$$

Fig 3.11 Schematic for Calculating Divergence

show that the laser intensity I and the distance h across the beam have the following relation:

For the HeNe laser:

D=2.35m $I=80.743\exp(-0.4725(h-3.10)^2)$ (μW)

D=5.84m $I=12.626\exp(-0.091(h-6.567)^2)$ (μW)

For the dye laser:

D=2.25m I=402.4exp(-2.044(h-1.506)^2) (μW)

D=5.47m I=62.83exp(-0.3786(h-2.832)^2) (μW)

From these fits the divergence of each beam can be calculated as shown in Fig 3.11. The divergence for the HeNe laser is $\theta=5.32\times10^{-4}$ rad and for the dye laser is $\theta=2.88\times10^{-4}$ rad.

The HeNe probe beam is loosely focused by a 20 cm focal length lens into the sample cell. The waist or focus size of the beam at the center of the cell was calculated from[56]:

$$w_2^2=w_1^2\left[1+\left(\frac{\lambda z}{\pi w_1^2}\right)^2\right]$$

$$R_1=z\left[1+\left(\frac{\pi w_1^2}{\lambda z}\right)^2\right]$$

$$\frac{1}{R_2}=\frac{1}{R_1}-\frac{1}{f}$$

$$w_0=\frac{f\lambda}{\pi w_2}$$

where f is the lens focal length. The parameters w_0, w_1, w_2, R_1, R_2 and z are shown in Fig 3.12. We determined that the HeNe beam is focused at 25.6 cm from the lens with a waist of about 100μm. This was confirmed by using a microscope to look at this point in the cell. The focus of the pump beam was then adjusted by L_4 in fig 3.1. A 40 cm focal length lens was used for L_4 to facilitate easy alignment and overlap of the laser beams. In previous work[39], both beams passed through both lenses making alignment and overlapping the beams difficult. Our scheme allows independent adjustment of both beams. The longer focal length lens still allows the pump beam to be focused at the correct place in the cell. By using two telescopes to view the focal region in the vertical

and horizontal directions we overlapped the beams, with the pump beam waist slightly larger than the probe beam waist.

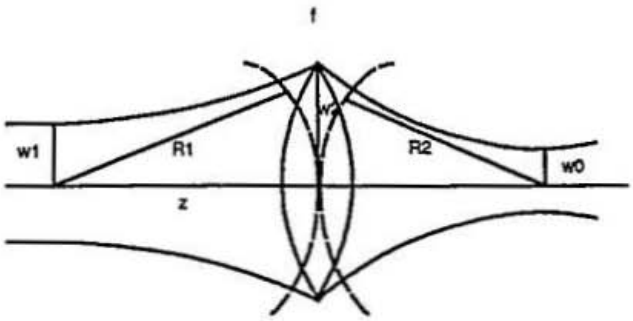

Fig 3.12. Imaging of a Gaussian Beam by a Thin Lens

3-5. Procedure for Collecting SBG Spectra

The procedure for collecting SBG spectra varied slightly, depending on the liquid sample used and the length of the scan. To collect spectra for CS_2, the dye laser was scanned with a speed of 10 MHz/sec and a step increment 10 MHz over a 20 GHz frequency region, containing both the gain and loss peaks. For CCl_4, we typically scanned

a 15 GHz region containing the loss and gain peaks. The laser scan speed was 20 MHz/sec with a step increment of 10 MHz. All spectra were taken with the samples at room temperature (20°C) and a 3S time constant for the lock-in amplifier. The autoscan data acquisition program collected data via 8 bit A/D converters, housed in a separate interface box. The data were normalized to the dye laser power to reduce the effects of pump laser power fluctuations. Once collected, data were viewed on the Apple screen where a cursor driven program can be used to determine the frequencies of any intensity features. The data were then transferred to an IBM PC computer from the Apple using an RS-232 interface set to 9600 baud. The data from the PC were typically viewed with commercial plotting routines. Because of the low resolution of the Apple screen, one of the drawbacks of our present setup is that we don't usually know how good the scan data are until we plot them on the PC computer.

3-6. Sample Preparation

Since the Brillouin gain signal is much weaker than the overall intensity of the probe beam, care must be taken to insure that samples are dust free. The liquid sample was filled into a quartz cell. Before the sample was introduced, the quartz cell was rinsed several times with acetone. When the cell had dried, the sample liquid was filtered under gravity through a 0.2μm teflon syringe filter and injected directly into the cell. The cell was rinsed this way several times and then filled and sealed with teflon caps. In our

experiments, the carbon disulfide is A.C.S reagent grade and the carbon tetrachloride is spectranalyzed A.C.S. grade.

CHAPTER 4.

EXPERIMENTAL RESULTS AND DISCUSSION

4-1. Carbon Disulphide (CS_2)

Fig 4.1 shows one representative sweep of the CW SBG spectra of liquid carbon disulfide. The sweep time of this spectrum was 2000 s. The spectrum is comprised mainly of the two Brillouin gain and loss peaks. The sharp Rayleigh peak in the center of the spontaneous Brillouin spectrum is absent as expected. The loss peak appears at lower pump frequencies and the gain peak appears at high pump frequencies. The loss peak corresponds to a loss in probe power as energy is transferred via phonons from the higher energy probe beam to the lower energy pump beam. The gain peak occurs when energy is transferred from the low energy probe beam to the higher energy pump beam. As can be seen from the plots, the signal-to-noise ratio is excellent in the SBG spectrum of this strong scattering sample.

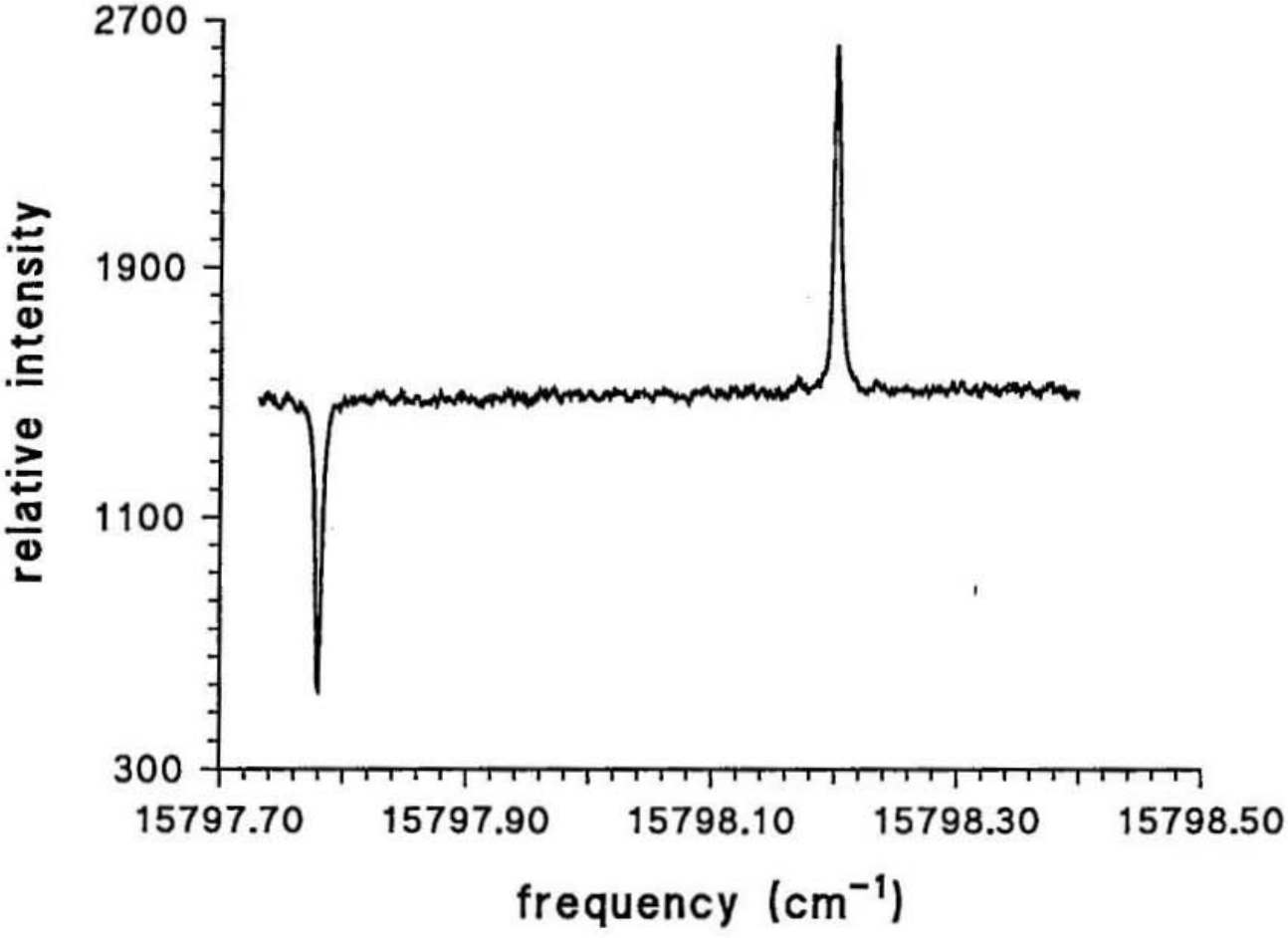

Fig. 4.1 Brillouin Gain Spectrum of CS_2

4-1-1. Measurement of Line Width, Brillouin Shift and Asymmetry Parameter

The effective laser linewidth of the dye laser is small enough (< 4 MHz) that accurate linewidth measurements of the BG signal can be made. In order to measure line widths and Brillouin shifts accurately, the loss and gain peaks are fitted by nonlinear least squares to the Lorentzian lineshape functions of the following form[40]:

$$G(\nu)=B\pm G^{0}\left(\frac{\Delta\nu_{B}}{(\nu-\nu_{G})^{2}+(\Delta\nu_{B})^{2}}+A\frac{(\nu-\nu_{G})}{(\nu-\nu_{G})^{2}+(\Delta\nu_{B})^{2}}\right) \quad . \qquad (4.1)$$

This function is Lorentzian in nature, but includes an asymmetry term characterized by the parameter A. This parameter characterizes the relative contribution of the Lorentzian and dispersive lineshapes to the experimental line shape.

The +(or -) sign refers to gain (or loss) peak, ν_G is the frequency of the gain or loss peak, $\Delta\nu_B$ is the width, in frequency units, of the Brillouin peak and G_0 is an intensity scaling factor to normalize the peak height to the experimental peak height. As expected, this function is maximum when $\nu=\nu_G$, i.e. when the frequency is at a gain or loss peak.

Fig 4.2 shows one of the fitting results. The Brillouin shift $\omega_B/2\pi$ was taken to be half the distance between the maxima of the gain and loss peaks. The half width $\Delta\nu_B$ and asymmetry factor A were taken to be the average of the gain and loss peaks values.

The lower trace in Fig4.2 is the difference between the experimental data and the

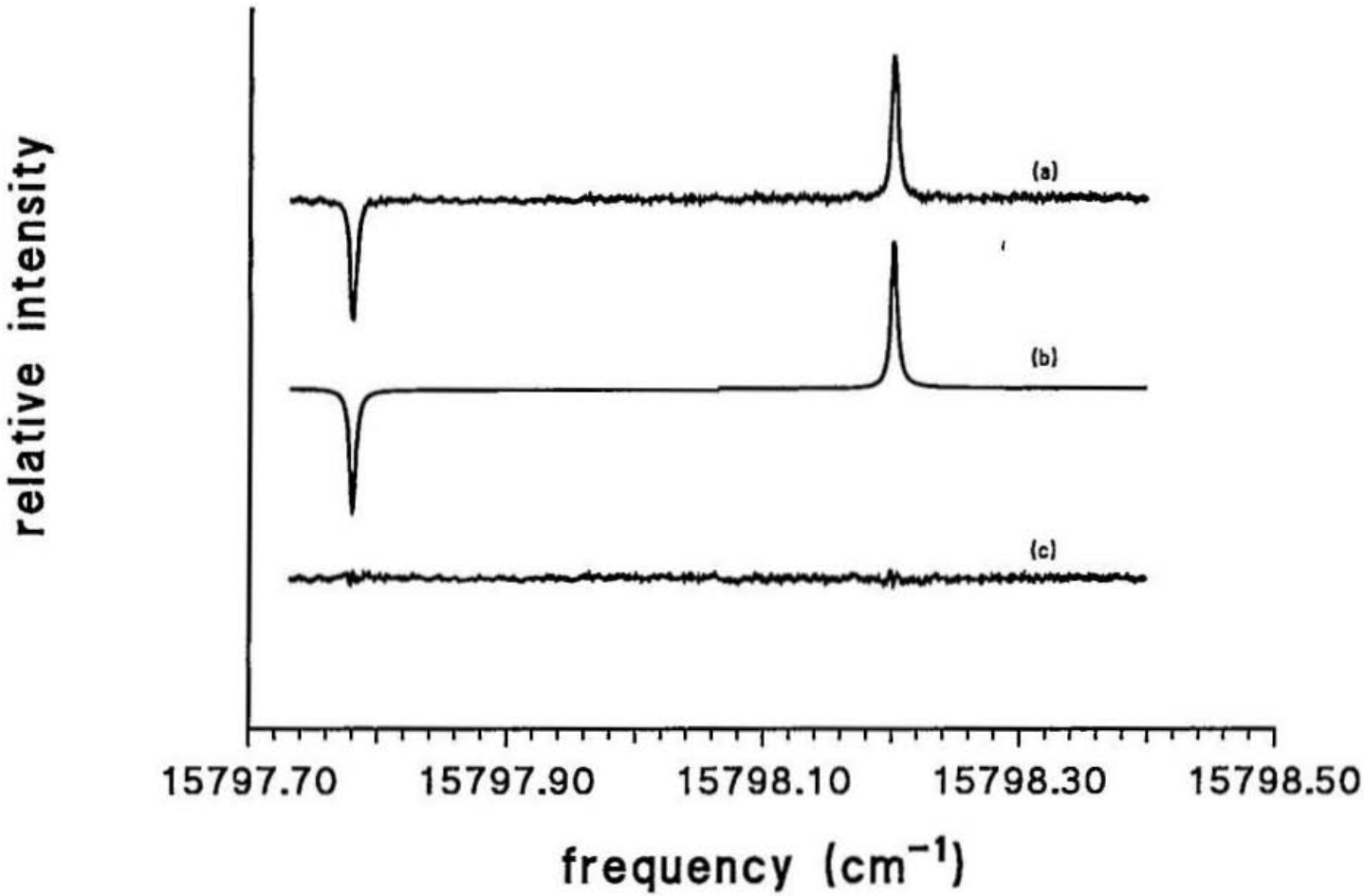

Fig 4.2 The Experimental BG Spectrum of CS_2 (trace a), the Fit of Lorentzian Function (trace b), and the Residuals from the Fit (trace c)

fitted one. The fit is very good except for a small derivative shaped feature at the gain and loss peak frequencies. This is most likely due to a deviation of the lineshape caused by the time constant used in the experiment. The remaining noise in this spectrum is due to stray pump laser light which gets through the lock-in filters.

The Brillouin shift, linewidth and asymmetry parameter were also determined for several other backscattering angles near 180°. The results, and the values from the literature are shown in Table 4.1. The literature results were measured by spontaneous Brillouin scattering, in a 90° scattering geometry, and have been corrected to the scattering wavevector used in our experiments. The consistency between our experimental results and literature results is good.

Substitution of the Brillouin shift and known value of the refractive index into eq(1.1) yields a value for the sound velocity in CS_2 of 1.209×10^5 cm/s, which is in good agreement with the previous result 1.241×10^5 cm/s[57].

Table 4.1. Experimental results for the Brillouin shift and half-linewidth at different scattering angles for CS_2

θ(degree)	experimental result			literature result
	$\omega_B/2\pi$(GHz)	$\Gamma_B/2\pi$(MHz)	A	$\omega_B/2\pi$(GHz)
179.5	6.40	117	0.062	6.41[58],6.36[59]
179.0	6.31	85	0.045	6.41, 6.36
176.9	6.39	110	0.054	6.41, 6.36
174.2	6.37	110	0.051	6.40, 6.35
172.0	6.39	133	0.12	6.39, 6.34

4-1-2. Absolute Gain

The absolute gain for CS_2 was estimated from the measurements of amplification of the probe beam and the change in the probe beam intensity. The current generated by the probe laser in one of the photodiodes was measured, and compared to the differential current generated at a gain peak. A value of 3.6×10^{-5} was obtained for the gain, which is consistent the value of 2×10^{-5} obtained by Ratanaphruks[39].

We have also calculated the absolute gain for the gain peak using equation (2.19).

$$G=\eta_c \frac{4\pi^3 c\omega_2}{\omega_1^3}\frac{\rho_0}{k_B T}[\Omega S(\vec{K},\Omega)]\frac{d\sigma}{d\Omega}P_2 \quad . \qquad (2.19)$$

To determine $S(\vec{K},\Omega)$, we note that CS_2 is a substance which relaxes with a single relaxation time. According to Mountain[57], for a single relaxation time process, the spontaneous scattering spectral density $S(\vec{K},\Omega)$ can be expressed as:

$$S(K,\Omega)=2\frac{N_1 D_1 + N_2 D_2}{D_1^2+D_2^2} \qquad (4.2)$$

where

$$N_1=-\Omega^2+ab_0K^4+c_0^2K^2(1-1/\gamma)+(ab_1K^4+b_1K^2\Omega^2\tau)/(1+\Omega^2\tau^2) \quad ,$$

$$N_2=\Omega[aK^2+b_0K^2+(b_1K^2-ab_1K^4\tau)/(1+\Omega^2\tau^2)] \ ,$$

$$D_1=-\Omega^2(aK^2+b_0K^2)+c_0aK^4/\gamma+(ab_1K^4\Omega^2\tau-\Omega^2b_1K^2)/(1+\Omega^2\tau^2) \quad ,$$

$$D_2=\Omega[-\Omega^2+c_0^2K^2+ab_0K^4+(b_1K^2\Omega^2\tau+ab_1K^4)/(1+\Omega^2\tau^2)] \ ,$$

K is the scattering wavevector, Ω is the difference frequency between the two lasers, and τ is the relaxation time of the medium. All the other constants a, b_0, c_0, b_1,Γ,n,γ were taken from Mountain[57]. Mountain has shown that this expression fits the spontaneous Brillouin spectra of CS_2 very well, indicating that it does indeed relax with a single relaxation time. By fitting S(K,Ω) and equation (2.19), we obtained a peak gain of 4.3×10^{-5}, which again is consistent with the above values.

4-1-3. Relation Between Gain Signal and Pump Power

Equation (2.19) is the expression for the gain in the steady state. In the steady state, the gain is linearly proportional to the pump intensity or power. If the interaction time is shorter than the characteristic time of the medium, the transient behaviour of the interaction must be considered[44, 45], and the gain becomes proportional to the square root of the pump intensity. In this work the laser modulation frequency was in the kHz range, corresponding to a modulation period of order 1 ms, and the relaxation time of the liquids studies was on the order of 1×10^{-9}-1×10^{-11} s. Our experiments easily fall into the steady state regime.

To test this dependence of signal on pump laser power, we have carried out a sequence of measurements of gain at different pump powers while keeping the other experimental parameters unchanged. The dependence of the relative gain, G, on the pump laser power, P_l, is shown in Figure 4.3.. It shows clearly that G is linearly proportional to P_l as equation (2.19) predicts. This linear dependence confirms that the interaction is in the steady state.

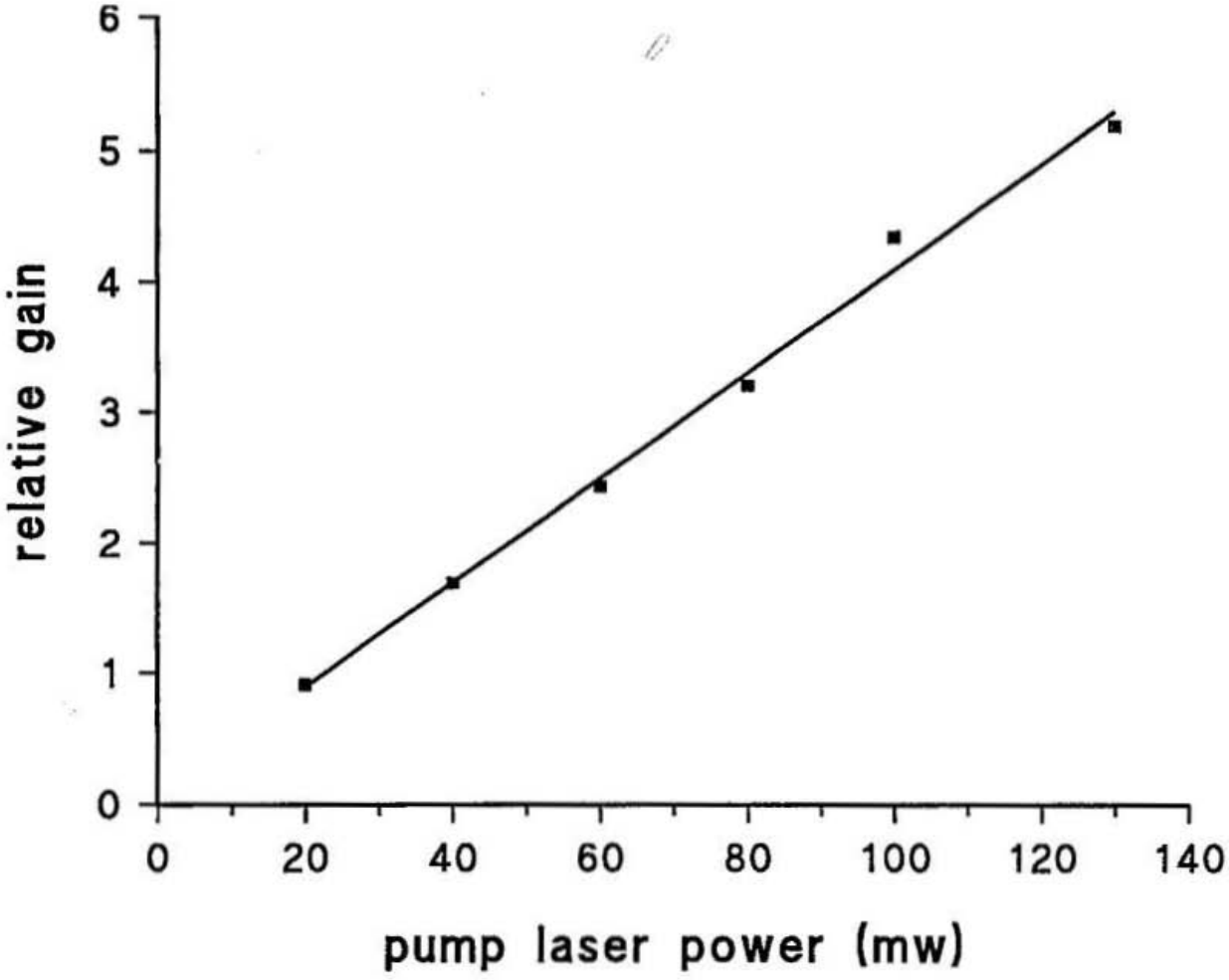

Fig 4.3. Relation between Gain and Pump Power

4-2. Carbon Tetrachloride (CCl_4)

Fig 4.4 (a) is a typical SBG spectra of carbon tetrachloride. The scan time of this spectrum was 750 s. The loss and gain peaks are clearly visible in the spectrum but the signal to noise ratio is degraded relative to the carbon disulfide spectrum.

4-2-1. Signal to Noise Ratio and Signal Averaging

The gain for CCl_4 was estimated at 2×10^{-6}, a factor of 10 less than the gain in CS_2. In order to enhance the signal to noise ratio, signal averaging was used. The autoscan program uniquely identifies the frequency of each data point to the precision of the wavemeter, allowing accurate addition of multiple data scans. To test the feasibitity of signal averaging we set the laser to a specific frequency just below the gain-loss region. The laser can be scanned over a short frequency (20 GHz) range by using a feature which tips only the thin etalon. The etalon then resets very accurately to the initial frequency. We collected the spectrum 16 times under the same conditions and added the spectra together. Fig 4.4(b) shows the final result. The signal to noise ratio is much improved. The larger amplitude fluctuations which are evident, especially in the flat portion of the spectrum, are due to slow power variations in the pump laser power as the dye laser was scanned in frequency. The small amplitude fluctuations, of very short deviation, correspond to random noise from other sourses

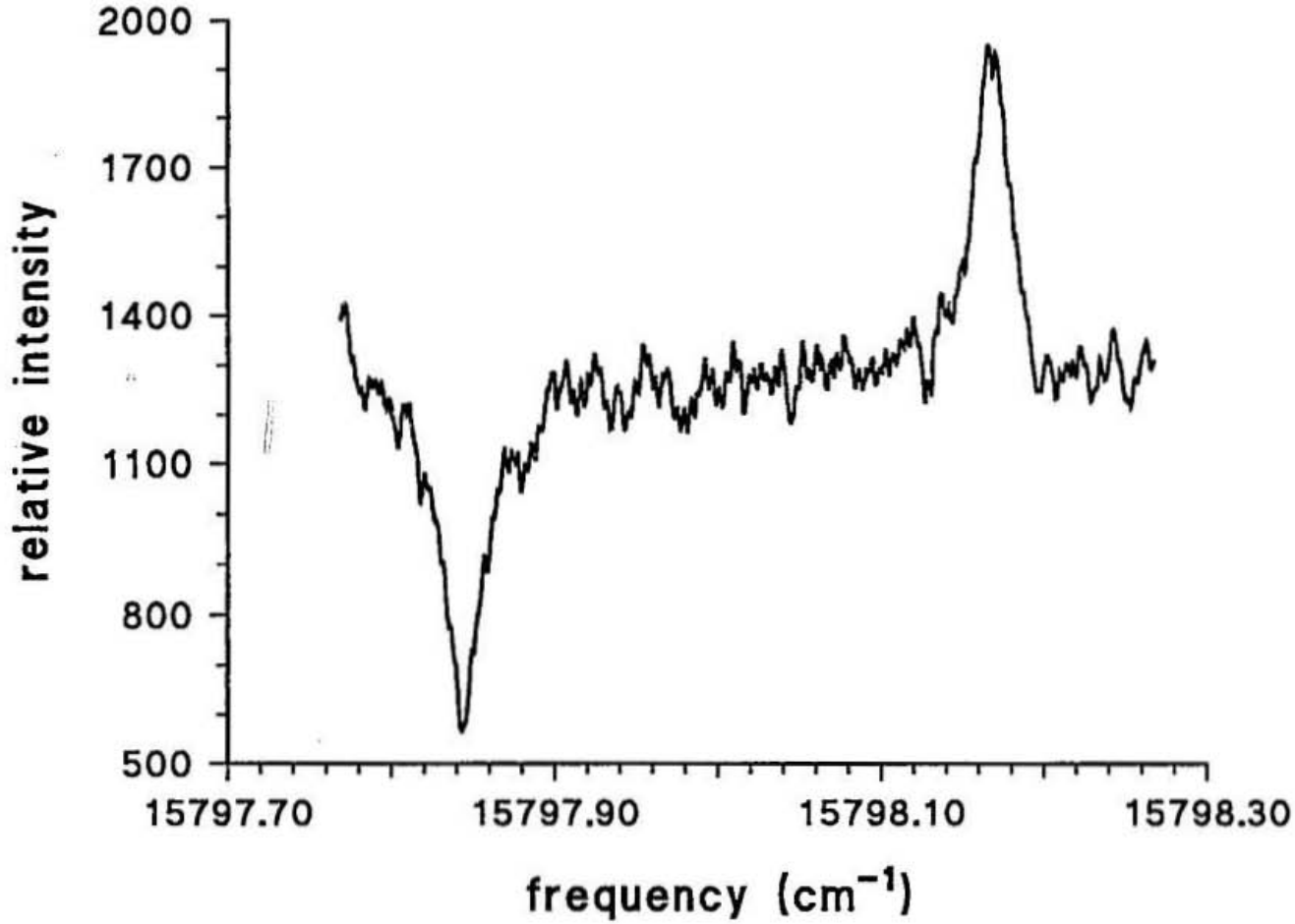

Fig 4.4 (a) Brillouin Gain Spectrum of CCl_4

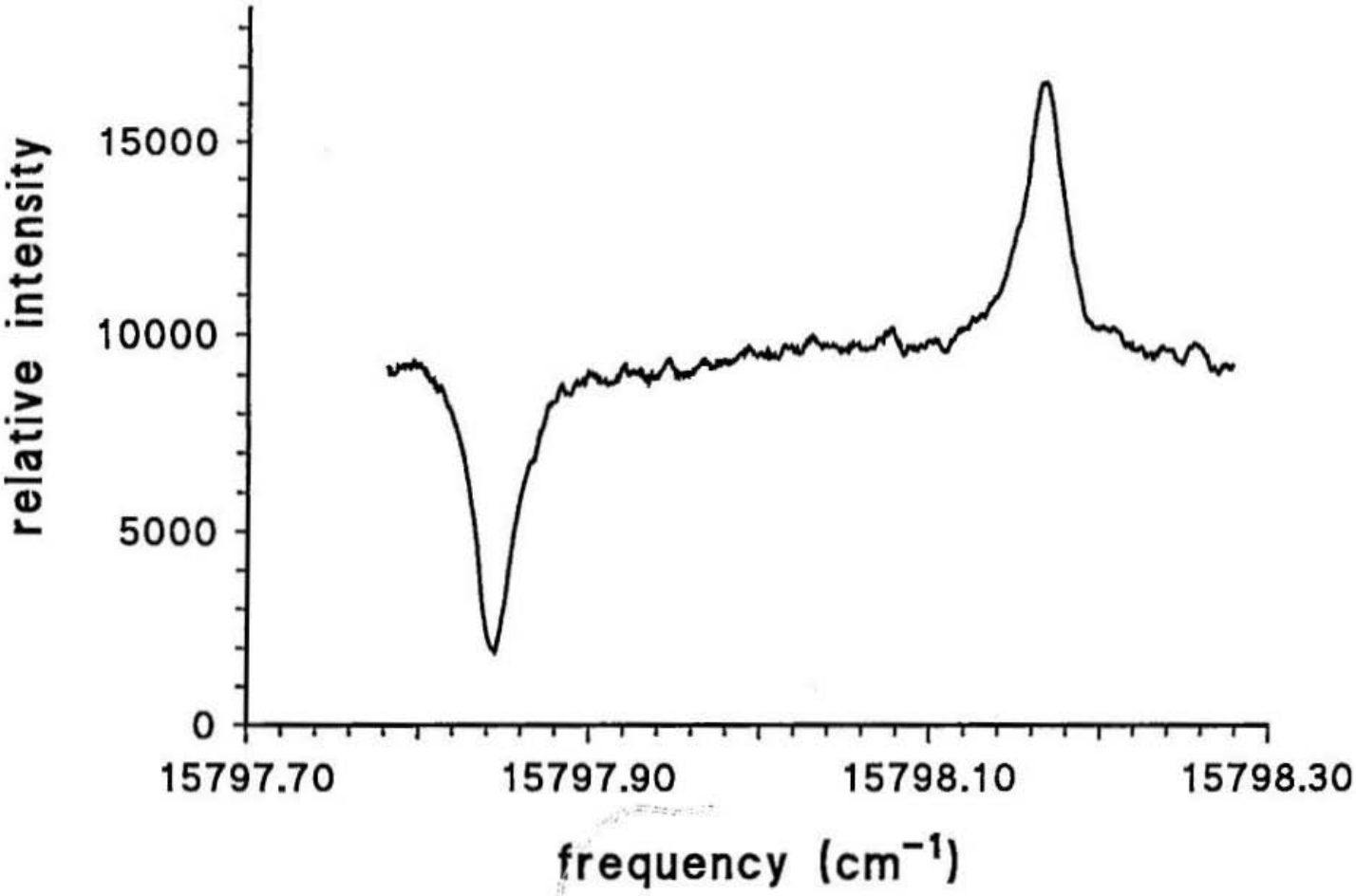

Fig 4.4 (b) Brillouin Gain Spectrum of CCl_4 after Using Signal Averaging

4-2-2. Line Width and Brillouin Shift

Using the same procedure as used for CS_2, the loss and gain peaks of CCl_4 were fitted to a lorentzian profile (eq(4.1)) using nonlinear least squares fitting. The result of such a fit is shown in Fig 4.5 and the fit is very good. The width of the Brillouin peak, $\Gamma_B=2\pi\Delta\nu_B$, and the Brillouin shift, $\omega_B/2\pi$, were determined from the fit. The Brillouin shift was taken to be half the distance between the maxima of the gain and loss peaks. The peak width was taken as the average value of the width of the gain and loss peak. It is clear from the data in table 4.2 that the agreement of the measured SBG shift from this work with the literature result is very good.

Table 4.2. Experimental result of CCl_4

parameter	present result	literature value[39]
Brillouin shift (GHz)	4.87	4.82
half width (MHz)	407	315

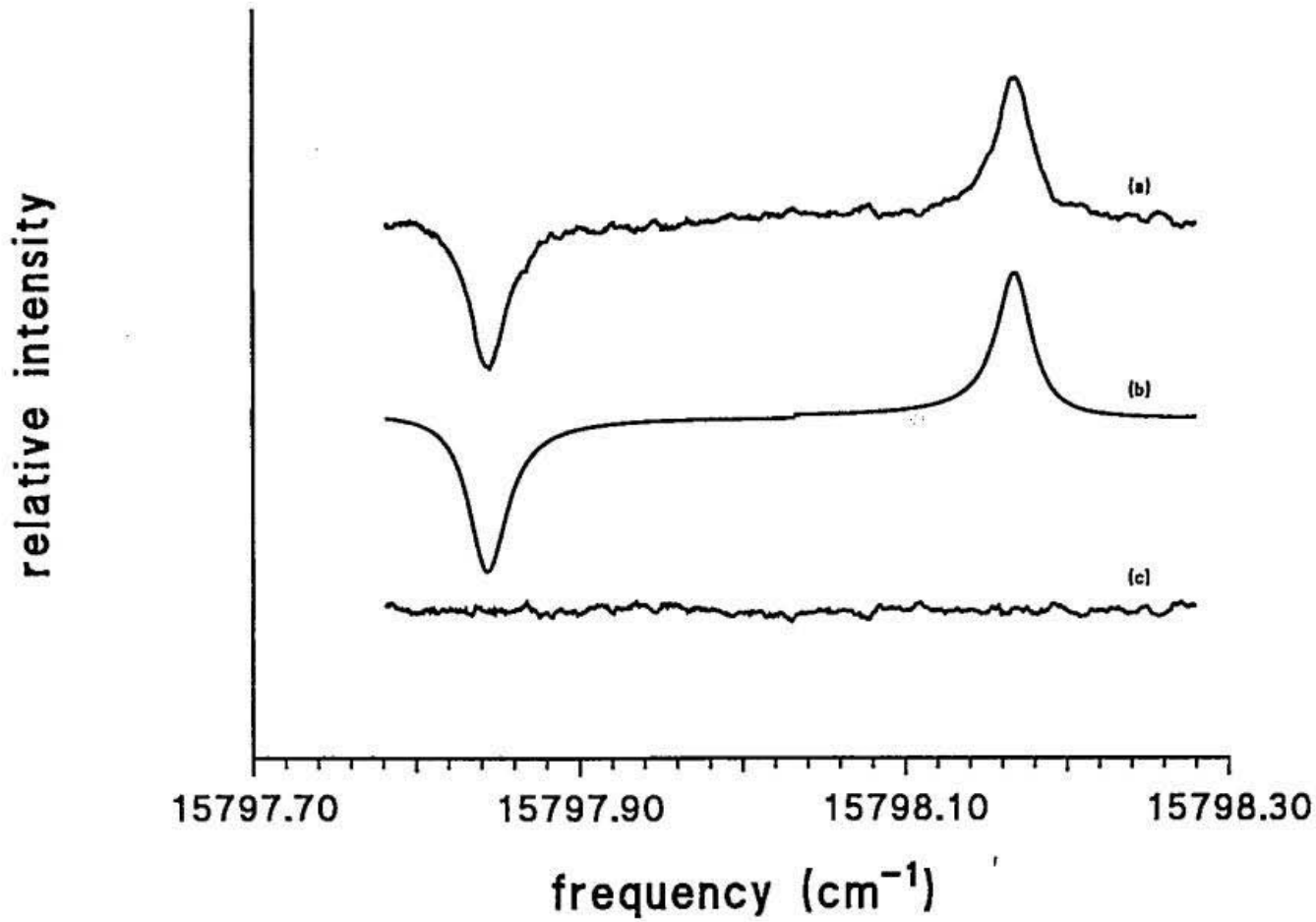

Fig 4.5 BG Spectrum of CCl_4 Signal Averaging Result(trace a), Fit for Lorentzian Function (trace b), and the Residuals from the Fit (trace c)

4-2-3. Mountain Mode

The SBG spectra of CS_2 and CCl_4 differ in several ways. The CS_2 peaks are much sharper and more intense than those in CCl_4. Furthermore the baseline between the two peaks in the CS_2 signal is very flat, whereas, the baseline in the CCl_4 signal shows a definite slope upward from the loss to the gain peak. This asymmetry is quite reproducible, and corresponds to the presence of the well-known Mountain mode [57, 60] in the spontaneous Brillouin spectrum.

The Mountain mode is a nonpropagating thermal mode, which relaxes with a time scale of the same order as the relaxation time τ of the liquid. Usually, in liquids, there are thermal and phonon modes which give rise to the central and two shifted Brillouin components. The spectral distribution can be expressed using eq(4.2). Mountain pointed out that a mode using a single relaxation time could not explain the Brillouin spectrum of CCl_4, and that another slow thermal mode must be present. This new mode results from the weak coupling of the internal degrees of freedom of the molecules to the translational degrees of freedom of the fluid and gives rise to density fluctuations. The affect on the spectral distribution is the appearance of a broad line at zero frequency. The observation that the SBG experiment has the sensitivity to detect the Mountain mode is particularly significant for applications of SBG spectroscopy to supercooled liquids[42, 61]. In supercooled liquids, structural relaxation processes cause a similar spectral feature. An accurate measurement of the shape of this feature can provide important information about these relaxation processes. This can complement the information from Brillouin shift and

linewidth measurements. We have fit the data shown in Fig 4.4 to the theoretical expression (eqs 4.2) given by Mountain using non-linear least squares fitting. The adjustable parameters were the center frequency of the spectrum, the position of the baseline and the height of the peaks. The results are shown in Fig 4.6. The sound velocity was calculated to be 898 m/s. It can be seen that the fit is very good, although not perfect. This can either be attributed to the uncertainty in some of the constants used, to a small experimental error or perhaps to the limited nature of the single relaxation time theory.

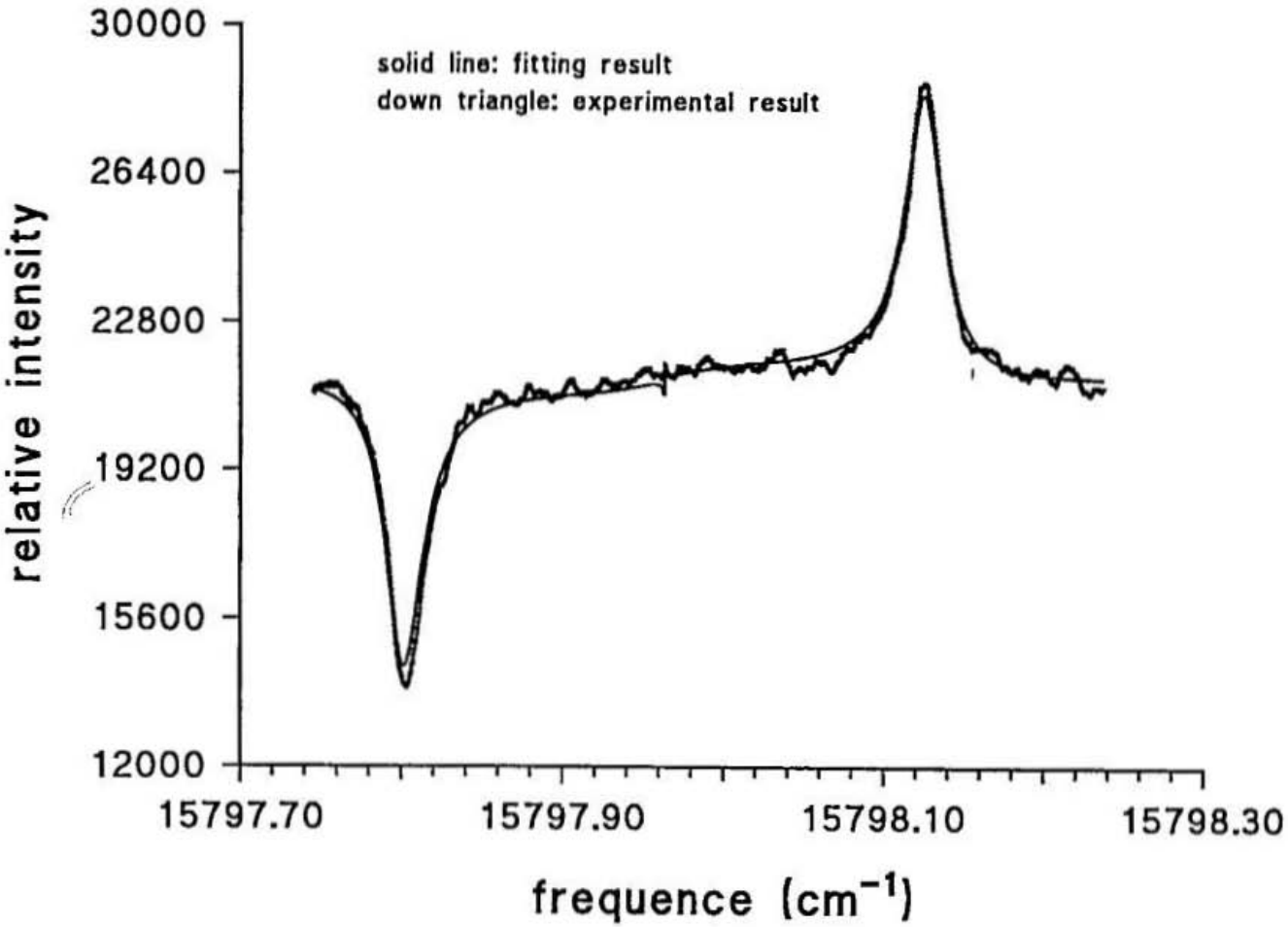

Fig 4.6. Fitting Result for CCl_4

4-3. Accuracy of Frequency and Linewidth Measurements

The frequencies of the Brillouin components were measured using the built-in wavemeter of the CR 699-29 ring dye laser. The wavemeter has an inherent uncertainty of 0.0005 cm^{-1} (15 MHz) which corresponds to the uncertainty in reading the high resolution part of the wavemeter (VET). The absolute frequency scale for the wavemeter was determined as outlined in sect. 3.2 by a calibration using the well known I_2 spectrum. The error in the standard spectrum[52] is (± 0.0025) cm^{-1} corresponding to an absolute frequency uncertainty of 75 MHz.

The accuracy of the linewidth measurements will be determined by the effective instrumental linewidth of our BG spectrometer and by the effect of $\vec{K}$ broadening due to the focusing of both laser beams. Although we have not accurately measured the effective instrumental linewidth, the linewidth in a similar system[38] was measured to be 7 MHz. It is reasonable to expect that our experimental linewidth is less than this. i.e., as mentioned before, to the order of 4 MHz

The $\vec{K}$ vector broadening is due to the angular spread of $\vec{K}$ vectors in the laser beam interaction region. This spread is caused by the focusing of the beams by the lens. The Brillouin shift is given as $\omega_b=v_b k$, where v_b is the sound velocity in the medium, so an uncertainty in $\vec{K}$ produces an uncertainty, i.e. broadening in the Brillouin line frequency. The uncertainty in $\vec{K}$ is given by[38]

$$\delta K=(2\cos\frac{\theta}{2})/w_{eff} \ ,$$

where θ is the scattering angle and w_{eff} is the spot size in the focal region. It is evident from this expression that $\vec{K}$ vector broadening is small for backward scattering and largest for forward scattering and that the more tightly focused the beam the greater the spread in the $\vec{K}$ vectors. The corresponding uncertainty in the frequency of the Brillouin peak is $\delta\nu=\frac{1}{2\pi}V_b\delta K$.

In our experimental setup a 20 cm focal length lens was used and produced a 100 μm beam waist in the centre of the focal region. Assuming a scattering angle of 179^0, the broadening is calculated to be about 36 KHz. In the backscattering geometry the CS_2 linewidths were typically 90 MHz, so this broadening can be considered insignificant. This type of broadening mechanism will be much more important in the forward scattering geometry where the linewidths are on the order of 10 MHz. For the same experimental parameters, and a scattering angle of 5^0, the uncertainty in linewidth due to $\vec{K}$ broadening is approximately 4 MHz, a significant fraction of the expected linewidth. We can conclude that in a backscattering geometry, $\vec{K}$ broadening effects are insignificant and measurements are limited by the instrumental linewidth of the spectrometer.

CHAPTER 5.

CONCLUSION

We have constructed a high resolution Brillouin gain spectrometer and demonstrated its usefulness in obtaining Brillouin gain signals in liquids. The BG spectra of a strong scatterer, carbon disulfide and a much weaker scatterer, carbon tetrachloride have been presented. In a 180^0 backscattering geometry the measured gains were 3.6×10^{-5} for CS_2 and 2×10^{-6} for CCl_4. These results are consistent with values reported in the literature.

The frequency resolution of this system is limited by jitter and the effective laser linewidths, and is less than 4MHz. In the recorded spectra the 85MHz wide Brillouin peaks of CS_2 were easily resolved, and the parameters associated with the asymmetry of the lineshape were determined. The BG spectra of CCl_4 clearly showed the asymmetry and sloping baseline associated with a slow thermal or Mountain mode in this liquid. The ability of this instrument to discern such subtle asymmetries is an indicator of its potential for these kinds of studies.

One of the major motivations underlying the construction of this apparatus was to eventually do temperature gradient studies of liquids, using a forward scattering geometry.

The absence of the Rayleigh peak in the SBG spectrum provides the possibility of observing such scattering at very small angles. In small angle or forward scattering the signal to noise ratio of the BG signal is much smaller than for the backscattering geometry. This lack of available signal to noise ratio demonstrates a serious limitation of our present spectrometer.

There are, however, several ways of improving the signal to noise ratio achievable with this system. It has been demonstrated by our results in CCl_4 that data acquisition by a computer lends itself to the possibility of the averaging of multiple scans and to a subsequent increase in the signal to noise ratio. In comparison to conventional Brillouin spectroscopy, where the addition of several thousand scans is not unusual, averaging should produce the same increases in signal to noise ratio in SBG spectroscopy. Since the Rayleigh peak is absent in this type of spectroscopy, an external Fabry-Perot could be used to generate frequency markers by which to overlap the scans properly.

The gain signal scales with the pump laser power so that the signal to noise ratio could be improved by increasing the pump laser power. One option would be to pulse amplify the output of the ring dye laser. The subsequent laser pulses would have the high peak power associated with a pulsed laser, yet the narrow linewidth associated with the CW ring dye laser.

The two major sources of noise in this experiment were amplitude fluctuations in the probe laser output and scattered pump light reaching the photodiodes. The probe laser power could be stabilized using an acousto-optic modulator and a polarizer in a feedback loop, much as is used in commercial instruments of this kind. Pump laser power reaching

the photodiodes might be less troublesome if the pump modulation frequency were far from the difference frequency. This could be achieved by using two AO modulators at, say, 20 and 50 KHz to modulate the lasers. With a lock-in Q of 100, the 50KHz signal would be about 70 Δf's away from the difference, as opposed to about 30 with our present setup.

Overlapping the pump and probe beams in the sample cell is another difficulty in the experiment. For example, in quartz, the scattering is so weak that we could not see the scattered light from the laser beams, and could not determine if the beams were overlapped. A method needs to be developed by which we can effectively overlap the laser beams independent of direct visual determination.

The high spectral resolution and narrow linewidth of the BG spectrometer should make it an idea tool for several types of Brillouin studies. As mentioned previously one of our primary interests is to study Brillouin scattering under the conditions of a large temperature gradient. It has been shown under such conditions the Brillouin lineshape should be asymmetric with the asymmetry parameter ε given by[62]

$$\varepsilon = \frac{v}{2\tau}\frac{\hat{q}\cdot\bar{\nabla}T}{T\cdot q^2}$$

where q is the wavevector of the scattering sound wave, $\bar{\nabla}T$ is the temperature gradient in the direction of $\hat{q}$, v is the sound velocity and Γ is the sound attenuation coefficient. The width of a Brillouin line is $2\Gamma\cdot q^2$.

It is important to note that this asymmetry is proportional to the temperature gradient $\bar{\nabla}T$ and inversely proportional to the scattering wavevector $\hat{q}$. This means that this effect will be greatest for small $\hat{q}$, i.e. in the forward scattering geometry, with large

temperature gradients present. There are two major limitations to carrying out this experiment using conventional Brillouin spectroscopy. First and foremost, the presence of a very strong Rayleigh peak in the spectrum, accompanied by a very small Brillouin shift make it difficult to see the very weak signal. Secondly, the small asymmetry in the linewidth is hard to measure with a Fabry-Perot interferometer. Nevertheless, two groups Beysens et al[63] and Kiefte et al[62] have carried out measurements on water. The results, though in reasonable agreement with the theoretical predictions for a liquid, indicate that a different experimental technique might be more appropriate to this problem.

The potential of SBG spectroscopy as a tool for investigating this problem is obvious. The absence of a Rayleigh line in the spectra and the narrow linewidth of the lasers make this technique attractive. The major obstacles to using this technique is the weakness of the BG signal in a forward scattering geometry. We feel that this can be overcome with the use of signal averaging techniques, as illustrated in our carbon tetrachloride data, and by refining our technique for overlapping the pump and probe beams. With these refinements to our system this spectrometer should be a powerful tool in temperature gradient work.

The second potential application of this spectrometer is the measurement of linewidths and asymmetry parameters in gases and liquids. The Brillouin linewidth in many liquids is often smaller than the instrumental linewidth of the FP's used in conventional Brillouin spectroscopy. With our apparatus we can make direct accurate linewidth measurements up to the resolution of the laser linewidth.

In conclusion, with signal averaging capabilities this spectrometer has the potential

to carry out high resolution Brillouin measurements, not achievable by other methods.

REFERENCES

1. L. Brillouin, *Ann. Physik* **17**, 88 (1922).
2. W. Hayes and R. Loudon, *Scattering of Light by Crystals*, (Wiley-Interscience, New York, 1978).
3. G.D. Patterson and A. Munoz-Rojas, *Ann. Rev. Phys. Chem.* **38**, 191 (1987).
4. P.A. Madden, *Light Scattering in Physics, Chemistry and Biology*, A.D. Buckingham, G.W. Series, E.R. Pike and J.G. Powles, Eds. (University Press, Cambridge, 1980), p209.
5. Y. Kato and G.A. Zdasiuk, *J. Opt. Soc. Am.* **65**, 995 (1975).
6. G.D. Patterson and P.J. Carroll, *J. Phys. Chem.* **89**, 1344 (1985).
7. M.M. Sushchinskiy, *Inelastic Light Scattering in Crystals (Translated by Allen, M.L.)*, Vol. 180, (Nova Science Publishers, Commack, 1987).
8. H.Z. Cummins and A.P. Levanyuk, *Light Scattering Near Phase Transitions*, (North-Holland, Amsterdam, 1983).
9. H.Z. Cummins, *Light Scattering in Physics, Chemistry and Biology*, A.D. Buckingham, G.W. Series, E.R. Pike and J.G. Powles, Eds. (University Press, Cambridge, 1980), p183.
10. I.L. Fabelinskii, *Molecular Scattering of Light*, (Plenum Press, New York, 1968).
11. B. Chu, *Laser Light Scattering*, (Academic Press, New York, 1974).

12. W. Kaiser and M. Maier, *Laser Handbook* (North-Holland, Amsterdam, 1972), p1077.

13. R. Pecora, *Dynamic Light Scattering*, (Plenum Press, New York, 1985).

14. L. Borjesson, M. Elmrothy and L.M. Torell, *Chem. Phys.* **149**, 209 (1990).

15. J.R. Sandercock, *Light Scattering in Solids*, M. Cardona and Güntherodt, Eds., Vol. III (Springer, Berlin, 1982), p173.

16. R. Mock, B. Hillebrands and R. Sandercock, *J. Phys.* **E20**, 656 (1986).

17. R. Vacher and J. Pelous, *Phys. Lett.* **53A**, 233 (1975).

18. R. Vacher and J. Pelous, *Phys. Rev.* **B14**, 823 (1976).

19. H. Sussner and R. Vacher, *Appl. Opt.* **18**, 3815 (1979).

20. J. Lorosch, J. Prlous and A. Levasseur, *J. Non-cryst. Solids* **69**, 1 (1985).

21. E. DiFabrizio, V. Mazzacurati, M. Nardone, A. Nucara, G. Ruocco and G. Signorelli, *J. Chem. Phys.* **93**, 7751 (1990).

22. E.J. Woodbury and W.K. Ng, *Proc.IRE* **50**, 2367 (1962).

23. A. Owyoung, *Opt. Commun.* **22**, 323 (1977).

24. R.Y. Chiao, C.H. Townes and B.P. Stoicheff, *Phys. Rev. Lett.* **12(21)**, 592 (1964).

25. E. Garmire and C.H. Townes, *Appl. Phys. Lett.* **5**, 84 (1964).

26. D. Pohl, M. Maier and W. Kaiser, *Phys. Rev. Lett.* **20**, 366 (1968).

27. D. Pohl and W. Kaiser, *Phys. Rev.* **B1**, 31 (1970).

28. M. Denariez and G. Bret, *Phys. Rev.* **171**, 160 (1968).

29. A.G. Jacobson and Y.R. Shen, *Appl. Phys. Lett.* **34**, 464 (1979).

30. M.D. Levenson, *Introduction to Nonlinear Laser Spectroscopy*, (Academic Press,

New York, 1982).

31. C.Y. She, G.C. Herring, H. Moosmuller and S.A. Lee, *Phys. Rev.* **31**, 3733 (1985).

32. C.Y. She, G.C. Herring, H. Moosmuller and S.A. Lee, *Phys. Rev. Lett.* **51**, 1648 (1985).

33. S.Y. Tang, C.Y. She and S.A. Lee, *Opt. Lett.* **12**, 870 (1987).

34. G.W. Faris, L.E. Jusinski, M.J. Dyer, W.K. Bischel and A.P. Hickman, *Opt. Lett.* **15**, 703 (1990).

35. G.W. Faris, L.E. Jusinski and A. Peet Hichman, *J. Opt. Soc. Am. B* **10**, 587 (1993).

36. N. Shibata, R.G. Waarts and R.P. Braun, *Opt. Lett.* **12**, 269 (1987).

37. W.T. Grubbs and R.A. MacPhail, *J. Chem. Phys.* **97**, 8906 (1992).

38. W.T. Grubbs and R.A. MacPhail, *J. Chem. Phys.* **97**, 19 (1992).

39. K. Ratanaphruks, W.T. Grubbs and R.A. MacPhail, *Chem. Phys.* **182**, 371 (1991).

40. W.T. Grubbs and R.A. MacPhail, *J. Phys. Chem.* **96**, 8688 (1992).

41. W.T. Grubbs and R.A. MacPhail, *Rev. Sci. Instrum.* **65**, 34 (1993).

42. W.T. Grubbs and R.A. MacPhail, *J. Chem. Phys.* **100(4)**, 2561 (1994).

43. I.L. Fabelinskii, D.I. Mash, V.V. Morozov and V.S. Starunov, *Phys. Lett.* **27a**, 253 (1968).

44. A. Yariv, *Quantum Electronics*, (3nd), (John Wiley & Sons, New York, 1989).

45. M. Sparks, *Phys. Rev. Lett.* **32**, 450 (1974).

46. Y.R. Shen, *Principles of Nonlinear Optics*, (Wiley-Interscience, New York, 1984).

47. M. Nelkin and A. Ghatak, *Phys. Rev.* **135**, a4 (1964).

48. T.F. Johnston Jr., R.H. Brady and W. Proffitt, *Appl. Opt.* **21**, 2307 (1982).

49. T.F. Johnston Jr., *Encyclopedia of Physical Science and Technology*, Vol. 14 (Academic Press, New York, 1987), p96.

50. G.H. Williams, J.L. Hobart and T.F.J. Johnston, S.I.C.O.L.S. Conference, Interlaken, Switzerland, June 29, p1-13 (1983).

51. O.G. Peterson, S.A. Tuccio and B.B. Snavely, *Appl. Phys. Lett.* **17**, 245 (1970).

52. S. Gerstenkorn and P. Luc, *Atlas du Spectre D'absorption de la Molécule D'iode 14,800 - 20,000 cm^{-1}*, (Imprimerie Louis-Jean, Paris, 1978).

53. M.S. Sorem and A.L. Schawlow, *Opt. Commun.* **5**, 148 (1972).

54. K.L. Jansen and J.M. Harris, *Appl. Spect.* **40**, 483 (1986).

55. M.D. Levenson and A.L. Schawlow, *Phys. Rev.* **6**, 10 (1972).

56. W. Demtroder, *Laser Spectroscopy (Basic Concepts and Instrumentation)*, (Springer-verlag Berlin Heidelberg, New York, 1981).

57. R.D. Mountain, *J. Res. Nat. Bur. Stand. - A: Phys. & Chem.* **70a**, 207 (1966).

58. H.Z. Cummins and K.W. Gammon, *J. Chem. Phys.* **44**, 2785 (1966).

59. D.P. Eastman, A. Hollinger and J. Kenemuth, *J. Chem. Phys.* **50**, 1567 (1969).

60. W.S. Gornall, G.I.A. Stegeman, B.P. Stoicheff, R.H. Stolen and V. Volterra, *Phys. Rev. Lett.* **17**, 297 (1966).

61. L. Borjesson, Elmroth.M and L.M. Torell, *Chem. Phys.* **149**, 209 (1990).

62. H. Kiefte, M.J. Clouter and R. Penney, *Phys. Rev.* **B30**, 4017 (1984).

63. D. Beysens, Y. Garrabons and G. Zalczer, *Phys. Rev. Lett.* **45**, 403 (1980).